Postprint of: Greś S., Riva R., Süleyman C. Y., Andersen P., Łuczak M., Uncertainty quantification of modal parameter estimates obtained from subspace identification: An experimental validation on a laboratory test of a large-scale wind turbine blade, ENGINEERING STRUCTURES Vol. 256 (2022), 114001, DOI: 10.1016/j.engstruct.2022.114001

Uncertainty quantification of modal parameter estimates obtained from subspace identification: an experimental validation on a laboratory test of a large-scale wind turbine blade

Szymon Greś [a,*], Riccardo Riva [b], Cem Yeniceli Süleyman [b], Palle Andersen [a], Marcin Mieczysław Łuczak [b,c]

[a] *Structural Vibration Solutions A/S, NOVI Science Park, 9220 Aalborg, Denmark*
[b] *DTU Wind Energy, Risø Campus, 4000 Roskilde, Denmark*
[c] *Gdańsk University of Technology, Faculty of Mechanical Engineering and Ship Technology, Narutowicza 11/12, 80-233 Gdańsk, Poland*

Abstract

The uncertainty afflicting modal parameter estimates stems from e.g., the finite data length, unknown, or partly measured inputs and the choice of the identification algorithm. Quantification of the related errors with the statistical Delta method is a recent tool, useful in many modern modal analysis applications e.g., damage diagnosis, reliability analysis, model calibration. In this paper, the Delta method-based uncertainty quantification methodology is validated for obtaining the uncertainty of the modal parameter and the modal indicator estimates in the context of several well-known subspace identification algorithms. The focus of this study is to validate the quality of each Delta method-based approximation with respect to the experimental Monte Carlo distributions of parameter estimates using a statistical distance measure. On top of that, the accuracy in obtaining the related confidence intervals is empirically assessed. The case study is based on data obtained from an extensive experimental campaign of a large scale wind turbine blade tested in a laboratory environment. The results confirm that the Delta method is, on average, adequate to characterize the distribution of the considered estimates solely based on the quantities obtained from one data set, validating the use of this statistical framework for uncertainty quantification in practice.

Keywords: Uncertainty quantification, subspace methods, operational modal analysis, experimental modal analysis, wind turbine blades

1. Introduction

The estimation of modal parameters from vibration measurements is the fundamental task in experimental testing of engineering structures. The practical value of the estimated parameters is significantly

*Corresponding author; *E-mail address: sg@svibs.com*

increased if the considered identification procedure provides a measure of their covariance. This information, however, is only useful when the underlying identification algorithm is consistent i.e., when the estimated parameters converge to their true values as the amount of data tends to infinity. Moreover, when the identification method yields asymptotically Gaussian distributed parameter estimates, information about their covariance is essential to derive the related confidence bounds, designating a range for the true (unknown) value of the parameter of interest. Few identification methods satisfy these requirements [1, 2]. Among them are subspace identification methods [3], whose aim is to identify system matrices of a linear time-invariant state-space model from input/output or output-only data. During the last decade, the subspace methods found a special interest in engineering applications for modal parameter estimation, see e.g., [4–15], due to their favorable statistical and numerical properties e.g., stationary [16] and non-stationary [17] consistency, asymptotic normality [16], and numerical efficiency in identification of large-scale systems [18].

The expressions for the asymptotic covariance related to the state-space matrices were first proposed in [19–22] and derived explicitly in [23]. The latter work allows directly to obtain the errors on the estimated state-space matrices by linking the covariance of the estimated parameters with the covariance of system states and innovation sequences. This approach, however, was only investigated on theoretical systems and not yet adopted to the modal analysis, since the computation of the unknown states and innovations, as well as the required noise covariances, is not necessary for the modal parameter estimation. A different approach was proposed in [24, 25], where the covariance of the estimated parameters is easily computed from the sample covariances of the vectorized data correlations and the related sensitivities, based on the first-order Delta method. Following this path, direct expressions to obtain the covariance related to the modal parameter estimates have been proposed for different members of the subspace method family e.g., output-only covariance-driven algorithm [17] in [25, 26], output-only data-driven algorithm in [27] and for input/output methods in [28–30]. These developments allowed the application of the modal parameter covariance estimates to various engineering problems e.g., damage diagnosis [31, 32], modal parameter tracking [11], model updating [33–36], and paved the way for the quantification of statistical uncertainties in the estimates of modal indicators i.e., Modal Phase Collinearity (MPC) [37] and Modal Assurance Criterion (MAC) [38].

The statistical Delta method-based uncertainty quantification methodology, however, still lacks a rigorous assessment of its accuracy in obtaining the confidence intervals of modal parameter and modal indicator estimates, shown e.g., in the context of a practical application to a large scale engineering structure. In the current paper, a simple statistical distance measure is applied to validate the Delta method-based framework

in the context of several well-known input/output and output-only subspace identification algorithms.

Compared to the validation study in [39], not only the Gaussian characteristics of the modal parameters are verified, but also the recently developed χ^2 approximation for the distribution of MAC and MPC estimates is confirmed in practice. Moreover, the present work focuses solely on the statistical variability of the parameters estimated from a single sensor configuration using several subspace algorithms, unlike [39], where the uncertainty of modal parameters with respect to measurements with different sensor configurations and for the output-only covariance-driven subspace identification method is considered. In addition, in contrast to [39] where a large number of in-situ tests of large-scale structures were employed, the current study is conducted on a large set of experimental data collected from a wind turbine blade tested in a laboratory environment. The correctness of the Delta method estimates is validated against an exhaustive Monte Carlo experiment, where the quality of the approximation with respect to the actual parameter distributions is verified for each Delta method-based distribution approximation. The practical benefit of such a validation is that it confirms that the statistical properties of modal parameter and modal indicator estimates obtained with Delta method are equivalent, in most of the cases, to the ones obtained from a taxing Monte Carlo experiment.

The paper is organized as follows. Some background on the system model is stated in Section 2. The identification methods used in this paper are recalled in Section 3. The uncertainty quantification strategy for the modal parameter estimates, the MAC and the MPC is given respectively in Section 4.1, Section 4.2 and Section 4.3. A validation of the obtained distribution approximations is enclosed in Section 5.

2. System modeling

The vibration behavior of a viscously damped, linear time-invariant structural system with m degrees of freedom is described by the differential equation

$$\mathcal{M}\ddot{q}(t) + \mathcal{C}\dot{q}(t) + \mathcal{K}q(t) = f(t) \tag{1}$$

where t denotes continuous time, and $\mathcal{M}, \mathcal{C}, \mathcal{K} \in \mathbb{R}^{m\times m}$ denote mass, damping and stiffness matrices, respectively. Vector $q(t) \in \mathbb{R}^m$ contains displacements and rotations at continuous-time degrees of freedom, here only the displacements are considered, and $f(t) \in \mathbb{R}^m$ comprises both measured and unmeasured external loads. Let system (1) be observed by sensors measuring, e.g., accelerations, velocities or displacements, at

r degrees of freedom (DOF) of the structure, collected in the vector

$$y(t) = C_a\ddot{q}(t) + C_v\dot{q}(t) + C_d q(t) + v(t) \tag{2}$$

where $y(t) \in \mathbb{R}^r$ is the output vector, $v(t) \in \mathbb{R}^r$ denotes the measurement noise, and matrices C_a, C_v, C_d $\in \mathbb{R}^{r\times m}$ select the respective type of the output at the measurement DOFs.

Sampled at time instants $t = k\tau$, where τ is the time step and k is an integer, (1) and (2) can be represented by a discrete-time innovation state-space model of order $n = 2m$

$$\widehat{x}_{k+1} = A\widehat{x}_k + Bu_k + K_k e_k \ , \tag{3}$$

$$y_k = C\widehat{x}_k + Du_k + e_k \ , \tag{4}$$

where $\widehat{x}_k \in \mathbb{R}^n$ are the state estimates corresponding to the non-stationary Kalman gain $K_k \in \mathbb{R}^{n\times n}$, $u_k \in \mathbb{R}^u$ denote the system inputs measured at u locations, and $\mathrm{E}(\widehat{x}_k - x_k) = 0$, where $\mathrm{E}(\cdot)$ denotes the expectation operator. The white noise innovations $e_k \in \mathbb{R}^n$ are one-step ahead prediction errors of y_k, given a past history of y_k and u_k.

The i-th natural frequency f_i, damping ratio ζ_i and the observed mode shape φ_i of the underlying structural system are related to the i-th eigenvalue $\lambda_i = \exp(\lambda_{ci}\tau)$ and the i-th eigenvector ϕ_i of A by

$$f_i = \frac{|\lambda_{ci}|}{2\pi},\ \zeta = \frac{-\Re(\lambda_{ci})}{|\lambda_{ci}|},\ \varphi_i = C\phi_i. \tag{5}$$

A mode shape having real, $\Re(\cdot)$, and imaginary, $\Im(\cdot)$, parts stacked, is defined as $\varphi_i^{\mathrm{R}} = \begin{bmatrix}\Re(\varphi_i)^T & \Im(\varphi_i)^T\end{bmatrix}^T$. The modal parameters are obtained from (A, C) whose identification can be achieved with e.g., subspace methods, which are revised next.

3. Subspace identification

One of the principal ideas in subspace identification is to combine the recursive equations of (3) into a single expression relating system matrices with data. To achieve that, subspace methods use the fact that a product of an observability matrix $\mathcal{O} = \begin{bmatrix}C^T & \cdots & (CA^{p-1})^T\end{bmatrix}^T \in \mathbb{R}^{pr\times n}$ with some state matrix $\widehat{\mathcal{X}}$ can be estimated from an adequate projection of a *past* and a *future* horizons of output or input/output data matrices, where p is a parameter that describes the size of the data horizon used. The purpose of this section is to concisely recall the main premise of the subspace algorithms applied in this work. Hereafter

it is assumed that inputs u are a realization of some stationary stochastic process persistently exciting the considered system [40], and that there is no feedback from y to u. A common step in every subspace identification algorithm is to define a data matrix containing a collection of p sequences spanning the past and the future of the available data.

Definition 1 (Data matrix). *Let $a_k \in \mathbb{R}^b$ be a discrete signal at time step k. For $0 \leq i \leq j \leq 2p-1$ the data matrix $\mathcal{A}_{i|j}$ writes*

$$\mathcal{A}_{i|j} = \frac{1}{\sqrt{N}} \begin{bmatrix} a_i & a_{i+1} & \dots & a_{i+N-1} \\ a_{i+1} & a_{i+2} & \dots & a_{i+N} \\ \vdots & \vdots & \vdots & \vdots \\ a_j & a_{j+1} & \dots & a_{j+N-1} \end{bmatrix} \in \mathbb{R}^{(j-i+1)b \times N}. \tag{6}$$

From the input and the output data, define the data matrices $\mathcal{Y}^- \in \mathbb{R}^{pr \times N}$, $\mathcal{Y}^+ \in \mathbb{R}^{pr \times N}$, $\mathcal{U}^- \in \mathbb{R}^{pu \times N}$, $\mathcal{U}^+ \in \mathbb{R}^{pu \times N}$

$$\mathcal{Y}^- = \mathcal{Y}_{0|p-1},\ \mathcal{Y}^+ = \mathcal{Y}_{p|2p-1},\ \mathcal{U}^- = \mathcal{U}_{0|p-1},\ \mathcal{U}^+ = \mathcal{U}_{p|2p-1},\ \mathcal{W}^- = \begin{bmatrix} \mathcal{U}^{-T} & \mathcal{Y}^{-T} \end{bmatrix}^T, \tag{7}$$

where $N + 2p$ is the number of available samples. Furthermore, denote the future block-row matrices for the Kalman states as $\widehat{\mathcal{X}}^+ = \widehat{\mathcal{X}}_{p|p}$. Data matrices $\mathcal{Y}^-$ and $\mathcal{Y}^+$ can be expressed by the recursion of (3)-(4) and with an adequate projection of either the output ($\mathcal{Y}^-, \mathcal{Y}^+$) or the input/output ($\mathcal{Y}^-, \mathcal{Y}^+, \mathcal{U}^-, \mathcal{U}^+$) data matrices, the estimated observability matrix $\widehat{\mathcal{O}}$, and the state sequence $\widehat{\mathcal{X}}$ can be factorized from a matrix $\widehat{\mathcal{H}}$

$$\widehat{\mathcal{H}} = \widehat{\mathcal{O}}\widehat{\mathcal{X}}\ . \tag{8}$$

This property has been shown for the data-driven subspace algorithms in many excellent work e.g., [3, 28], and is recalled in the context of several identification algorithms in the next section.

3.1. Identification algorithms

A key step in subspace identification is the estimation of the observability matrix $\mathcal{O}$ from $\widehat{\mathcal{H}}$, where different data projection methods can lead to either covariance or data-driven algorithms to obtain $\widehat{\mathcal{H}}$. For the covariance-driven methods, $\widehat{\mathcal{H}}$ is related to the auto and cross-covariance matrices of the available data i.e., products of (7) with their transposes. For the data-driven methods, $\widehat{\mathcal{H}}$ relates to a projection of data matrices with data matrices. Both the covariance-driven and the data-driven identification algorithms can yield consistent estimates of $\mathcal{O}$ [16, 17, 21], however for a finite amount of data obtained estimates are

subjected to statistical errors i.e., variance and bias. Those errors are method-dependent and propagate to estimates of (A, C), and consequently to the estimates of modal parameters. Analysis and comparison of the variance errors stemming from different identification methods, is the subject of this paper. For this purpose, four projection algorithms to obtain $\widehat{\mathcal{H}}$ are analyzed, namely

- the input/output covariance-driven algorithm in Section 3.1.1,
- the input/output data-driven oblique projection algorithm in Section 3.1.2,
- the output-only covariance-driven algorithm in Section 3.1.3,
- the output-only data-driven orthogonal projection algorithm in Section 3.1.4,

and two approaches to estimate (A, C) are considered for the data-driven output-only identification algorithm. For each projection algorithm, $\widehat{\mathcal{O}}$ can be retrieved from $\widehat{\mathcal{H}}$ by an SVD truncated at model order n

$$\widehat{\mathcal{H}} = \begin{bmatrix} \widehat{U}_{\mathrm{s}} & \widehat{U}_{\mathrm{ker}} \end{bmatrix} \begin{bmatrix} \widehat{D}_{\mathrm{s}} & 0 \\ 0 & \widehat{D}_{\mathrm{ker}} \end{bmatrix} \begin{bmatrix} \widehat{V}_{\mathrm{s}}^T \\ \widehat{V}_{\mathrm{ker}}^T \end{bmatrix} \tag{9}$$

and

$$\widehat{\mathcal{O}} = \widehat{U}_{\mathrm{s}} \widehat{D}_{\mathrm{s}}^{1/2}, \tag{10}$$

where $\widehat{U}_{\mathrm{s}} \in \mathbb{R}^{pr \times n}$ contains the left singular vectors, $\widehat{D}_{\mathrm{s}} \in \mathbb{R}^{n \times n}$ contains the non-zero singular values and $\widehat{V}_{\mathrm{s}} \in \mathbb{R}^{pr \times n}$ contains the right singular vectors. A naive approach to obtain the orthogonal projection of a data matrix $\mathcal{A}$ onto the orthogonal complement of $\mathcal{B}$ writes as $\mathcal{A}/\mathcal{B}^{\perp} = \mathcal{A} - \mathcal{A}/\mathcal{B} = \mathcal{A} - \mathcal{A}\mathcal{B}^T(\mathcal{B}\mathcal{B}^T)^{-1}\mathcal{B}$. An efficient and numerically stable implementation of the latter is obtained with QR factorization, which is detailed e.g., in [3].

3.1.1. Input/output covariance-driven algorithm

The first approach uses an orthogonal projection of $\mathcal{Y}^+$ onto $\mathcal{U}^+$, right-multiplied with the past output data matrix $(\mathcal{Y}^-)^T$, and is defined after [28] as

$$\widehat{\mathcal{H}}_{\mathrm{IOcov}} = (\mathcal{Y}^+/\mathcal{U}^{+\perp})(\mathcal{Y}^-)^T = \widehat{\mathcal{O}}\widehat{\mathcal{X}}^+_{\mathrm{IOcov}} \ , \tag{11}$$

where $\widehat{\mathcal{X}}^+_{\mathrm{IOcov}} = (\widehat{\mathcal{X}}^+/\mathcal{U}^{+\perp})(\mathcal{Y}^-)^T$.

3.1.2. Input/output data-driven oblique projection algorithm

The second method uses an oblique projection of $\mathcal{Y}^+$ onto $\mathcal{W}^-$ along $\mathcal{U}^+$ and is known in the literature as N4SID algorithm [41]. The resultant projection matrix $\widehat{\mathcal{H}}_{\mathrm{IOdat}}$ writes

$$\widehat{\mathcal{H}}_{\mathrm{IOdat}} = \mathcal{Y}^+ /_{\mathcal{U}^+} \mathcal{W}^- = (\mathcal{Y}^+ / \mathcal{U}^{+\perp})(\mathcal{W}^- / \mathcal{U}^{+\perp})^\dagger \mathcal{W}^- = \widehat{\mathcal{O}} \widehat{\mathcal{X}}^+_{\mathrm{IOdat}} \ , \tag{12}$$

where $\widehat{\mathcal{X}}^+_{\mathrm{IOdat}} = \widehat{\mathcal{X}}^+_{\mathrm{IOcov}} (\mathcal{W}^- / \mathcal{U}^{+\perp})^\dagger \mathcal{W}^-$ is defined in detail in [41] and $(\cdot)^\dagger$ denotes the Moore-Penrose pseudoinverse.

3.1.3. Output-only covariance-driven algorithm

The third method is an output-only covariance-driven algorithm, where the estimate of $\mathcal{O}$ is factored as

$$\widehat{\mathcal{H}}_{\mathrm{OOcov}} = \mathcal{Y}^+ \mathcal{Y}^{-T} = \widehat{\mathcal{O}} \widehat{\mathcal{X}}^+_{\mathrm{OOcov}} \ , \tag{13}$$

where $\widehat{\mathcal{X}}^+_{\mathrm{OOcov}} = \widehat{\mathcal{X}}^+ \mathcal{Y}^{-T}$.

3.1.4. Output-only data-driven orthogonal projection algorithm

The fourth approach uses an orthogonal projection of the row space of $\mathcal{Y}^+$ onto the row space of $\mathcal{Y}^-$, and is known in the literature as data-driven UPC algorithm [3]

$$\widehat{\mathcal{H}}_{\mathrm{OOdat}} = \mathcal{Y}^+ / \mathcal{Y}^- = \widehat{\mathcal{O}} \widehat{\mathcal{X}}^+_{\mathrm{OOdat}} \ , \tag{14}$$

where $\widehat{\mathcal{X}}^+_{\mathrm{OOdat}} = \widehat{\mathcal{X}}^+ / \mathcal{Y}^-$.

3.2. Estimation of (A, C)

Two methods to estimate (A, C) are used in this work. First, consider computing $(\widehat{A}, \widehat{C})$ directly from $\widehat{\mathcal{O}}$. An estimate of the observation matrix C is obtained from the first block-row of $\widehat{\mathcal{O}}$. The state transition matrix A is estimated from the shift invariance property of $\widehat{\mathcal{O}}$, namely $\widehat{A} = \underline{\widehat{\mathcal{O}}}^\dagger \overline{\widehat{\mathcal{O}}}$, where $\overline{\widehat{\mathcal{O}}}, \underline{\widehat{\mathcal{O}}} \in \mathbb{R}^{(p-1)r \times n}$ are respectively the matrix $\widehat{\mathcal{O}}$ without the first and the last block rows. Second, matrices $(\widehat{A}, \widehat{C})$ are obtained from the regression of shifted state sequences. This is explained in detail in [3]. Note that while the first approach is universal for every algorithm recalled in Sections 3.1.1-3.1.4, the second approach yields consistent estimates of (A, C) for the output-only data-driven UPC projection method from Section 3.1.4 but not for the input-output data-driven oblique projection algorithm from Section 3.1.2 [3].

4. Uncertainty quantification

The covariance related to the modal parameter estimates can be obtained with the first-order Delta method, which is a statistical tool to derive an approximate probability distribution for a function of an asymptotically Gaussian variable by using the first-order Taylor series approximation of that function [42]. The validity of its application stems from the fact that modal parameters estimated with the subspace algorithms can be expressed as a function of data covariance matrices, which are asymptotically Gaussian distributed [43], and are easy to compute. Then, the first-order Delta method is used to propagate the sample covariance of data covariance estimates onto modal parameter estimates, through all the steps of the chosen identification algorithm. Therefore, the covariance of the modal parameters can be evaluated directly from a single set of measurements and their statistical distribution is, in theory, asymptotically Gaussian.

The link between the data covariance matrices and the modal parameters is established with sensitivity matrices. These matrices are derived with the perturbation theory and depend on the chosen identification algorithm. The purpose of this section is to sketch the general principles of the first-order Delta method-based scheme for uncertainty quantification of modal parameters, which will be applied in the next section.

4.1. Covariance of modal parameter estimates

Let $\widehat{\mathcal{R}}_1, \ldots, \widehat{\mathcal{R}}_{11}$ be the data covariance matrices computed on N data samples as

$$\widehat{\mathcal{R}}_1 = \mathcal{Y}^+\mathcal{Y}^{+T}, \;\; \widehat{\mathcal{R}}_2 = \mathcal{Y}^+\mathcal{Y}^{-T}, \;\; \widehat{\mathcal{R}}_3 = \mathcal{Y}^-\mathcal{Y}^{-T}, \;\; \widehat{\mathcal{R}}_4 = \mathcal{Y}^+\mathcal{U}^{+T}, \;\; \widehat{\mathcal{R}}_5 = \mathcal{Y}^-\mathcal{U}^{+T}, \;\; \widehat{\mathcal{R}}_6 = \mathcal{Y}^+\mathcal{U}^{-T},$$
$$\widehat{\mathcal{R}}_7 = \mathcal{Y}^-\mathcal{U}^{-T}, \;\; \widehat{\mathcal{R}}_8 = \mathcal{U}^+\mathcal{U}^{+T}, \;\; \widehat{\mathcal{R}}_9 = \mathcal{Y}^+\mathcal{W}^{-T}, \;\; \widehat{\mathcal{R}}_{10} = \mathcal{W}^-\mathcal{U}^{+T}, \;\; \widehat{\mathcal{R}}_{11} = \mathcal{W}^-\mathcal{W}^{-T},$$

and let $\mathcal{R}_1, \ldots, \mathcal{R}_{11}$ be their respective theoretical (exact) counterparts. Next, denote $\text{vec}(\widehat{\mathcal{R}})$ as an array stacking a subset of $\widehat{\mathcal{R}}_1, \ldots, \widehat{\mathcal{R}}_{11}$ of the matrices required for a chosen subspace method, where $\text{vec}(\cdot)$ is the column-stacking vectorization operator. The $\text{vec}(\widehat{\mathcal{R}})$ is an estimate of the exact (unknown) $\text{vec}(\mathcal{R})$ and satisfies the Central Limit Theorem (CLT) [28, 43]

$$\sqrt{N}(\text{vec}(\widehat{\mathcal{R}}) - \text{vec}(\mathcal{R})) \to \mathcal{N}(0, \Sigma_{\mathcal{R}}), \tag{15}$$

where $\Sigma_{\mathcal{R}}$ is the asymptotic covariance of $\text{vec}(\widehat{\mathcal{R}})$ containing auto and cross-covariance matrices of the chosen subset of $\widehat{\mathcal{R}}_1, \ldots, \widehat{\mathcal{R}}_{11}$.

The choice of covariance matrices contained in $\text{vec}(\widehat{\mathcal{R}})$ relates to the choice of the data projection algorithm used to compute $\widehat{\mathcal{H}}$ [28]. In case of the covariance-driven algorithms (11) and (13), $\widehat{\mathcal{H}}$ can be expressed

as

$$\widehat{\mathcal{H}}_{\mathrm{IOcov}} = \widehat{\mathcal{R}}_2 - \widehat{\mathcal{R}}_4\widehat{\mathcal{R}}_8^{\dagger}\widehat{\mathcal{R}}_5^T \quad \text{and} \quad \widehat{\mathcal{H}}_{\mathrm{OOcov}} = \widehat{\mathcal{R}}_2.$$

For the data-driven algorithms (12) and (14), $\widehat{\mathcal{H}}$ depends not only on the data covariance matrices but also on the data matrices. This is problematic for uncertainty propagation, since $\widehat{\mathcal{H}}$ does not converge to a fixed limit as the number of its columns increases with the sample size. However, the estimates of (A, C) (as well as modal parameter estimates) would be equivalent if obtained from the "square" matrix $\widehat{\mathcal{H}}^s = \widehat{\mathcal{H}}\widehat{\mathcal{H}}^T$ [28]. Thus, their uncertainties can be derived from $\widehat{\mathcal{H}}^s$ that is related directly to the data covariance matrices as

$$\widehat{\mathcal{H}}^s_{\mathrm{IOdat}} = \widehat{\mathcal{H}}_{\mathrm{IOdat}}\widehat{\mathcal{H}}^T_{\mathrm{IOdat}} = \widehat{\mathcal{Z}}_1\widehat{\mathcal{Z}}_2^{\dagger}\widehat{\mathcal{R}}_{11}\widehat{\mathcal{Z}}_2^{\dagger}\widehat{\mathcal{Z}}_1^T \quad \text{and} \quad \widehat{\mathcal{H}}^{\mathrm{s}}_{\mathrm{OOdat}} = \widehat{\mathcal{H}}_{\mathrm{OOdat}}\widehat{\mathcal{H}}^{\mathrm{T}}_{\mathrm{OOdat}} = \widehat{\mathcal{R}}_2\widehat{\mathcal{R}}_3^{\dagger}\widehat{\mathcal{R}}_2^{\mathrm{T}},$$

where $\widehat{\mathcal{Z}}_1 = \mathcal{R}_9 - \mathcal{R}_4\mathcal{R}_8^{\dagger}\mathcal{R}_{10}^T$ and $\widehat{\mathcal{Z}}_2 = \mathcal{R}_{11} - \mathcal{R}_{10}\mathcal{R}_8^{\dagger}\mathcal{R}_{10}^T$. Subsequently, as $\widehat{\mathcal{H}}$ can be expressed as a function of $\widehat{\mathcal{R}}$, its first-order Taylor expansion writes as

$$\mathrm{vec}(\widehat{\mathcal{H}}) \approx \mathrm{vec}(\mathcal{H}) + \mathcal{J}_{\mathcal{R}}^{\mathcal{H}}(\mathrm{vec}(\widehat{\mathcal{R}}) - \mathrm{vec}(\mathcal{R})), \tag{16}$$

where $\mathcal{J}_{\mathcal{R}}^{\mathcal{H}}$ is a a non-zero first-order derivative of $\mathcal{H}$ w.r.t. $\mathcal{R}$ and $\mathcal{H}$ is the limit of $\widehat{\mathcal{H}}$. Delta method states that an associated CLT holds for $\mathrm{vec}(\widehat{\mathcal{H}})$ as

$$\sqrt{N}(\mathrm{vec}(\widehat{\mathcal{H}}) - \mathrm{vec}(\mathcal{H})) \to \mathcal{N}(0, \Sigma_{\mathcal{H}})$$

where the asymptotic covariance $\Sigma_{\mathcal{H}} = \mathcal{J}_{\mathcal{R}}^{\mathcal{H}}\Sigma_{\mathcal{R}}(\mathcal{J}_{\mathcal{R}}^{\mathcal{H}})^T$. This allows to propagate the covariance related to $\widehat{\mathcal{R}}$ to $\widehat{\mathcal{H}}$, or to any other quantity obtained from $\widehat{\mathcal{R}}$. Consistent estimates of the sensitivity $\mathcal{J}_{\mathcal{R}}^{\mathcal{H}}$ and the covariance $\Sigma_{\mathcal{R}}$ are required for the estimation of $\Sigma_{\mathcal{H}}$. The sensitivity $\mathcal{J}_{\mathcal{R}}^{\mathcal{H}}$ is consistently estimated with the first-order perturbation $\mathrm{vec}(\Delta\mathcal{H}) \approx \mathcal{J}_{\mathcal{R}}^{\mathcal{H}}\mathrm{vec}(\Delta\mathcal{R})$, where $\Delta\mathcal{H} = \widehat{\mathcal{H}} - \mathcal{H}$ and $\Delta\mathcal{R} = \widehat{\mathcal{R}} - \mathcal{R}$. A consistent estimate of $\Sigma_{\mathcal{R}}$ can be easily obtained from a sample covariance, as detailed in [28]. It follows that, the asymptotic covariance of $\mathrm{vec}(\widehat{\mathcal{H}})$ is consistently approximated by $\widehat{\Sigma}_{\mathcal{H}} = \mathrm{vec}(\Delta\mathcal{H})\mathrm{vec}(\Delta\mathcal{H})^T = \mathcal{J}_{\mathcal{R}}^{\mathcal{H}}\widehat{\Sigma}_{\mathcal{R}}(\mathcal{J}_{\mathcal{R}}^{\mathcal{H}})^T$.

With these tools, the covariance of $\widehat{\mathcal{R}}$ is propagated through all the steps of the chosen identification

algorithm and onto the i-th modal parameter estimate $\widehat{f}_i$, $\widehat{\zeta}_i$, $\widehat{\varphi}_i^{\mathrm{R}}$, based on the relation

$$\Delta f_i \approx \mathcal{J}_{\mathcal{H}}^{f_i} \mathcal{J}_{\mathcal{R}}^{\mathcal{H}} \mathrm{vec}(\Delta\mathcal{R}), \quad \widehat{\sigma}_{f_i}^2 = \Delta f_i (\Delta f_i)^T, \tag{17}$$

$$\Delta \zeta_i \approx \mathcal{J}_{\mathcal{H}}^{\zeta_i} \mathcal{J}_{\mathcal{R}}^{\mathcal{H}} \mathrm{vec}(\Delta\mathcal{R}), \quad \widehat{\sigma}_{\zeta_i}^2 = \Delta \zeta_i (\Delta \zeta_i)^T, \tag{18}$$

$$\Delta \varphi_i^{\mathrm{R}} \approx \mathcal{J}_{\mathcal{H}}^{\varphi_i^{\mathrm{R}}} \mathcal{J}_{\mathcal{R}}^{\mathcal{H}} \mathrm{vec}(\Delta\mathcal{R}), \quad \widehat{\Sigma}_{\varphi_i^{\mathrm{R}}} = \Delta \varphi_i^{\mathrm{R}} (\Delta \varphi_i^{\mathrm{R}})^T, \tag{19}$$

where $\mathcal{J}_{\mathcal{H}}^{f_i}$, $\mathcal{J}_{\mathcal{H}}^{\zeta_i}$ and $\mathcal{J}_{\mathcal{H}}^{\varphi_i^{\mathrm{R}}}$ are the real-valued sensitivity matrices of the chosen modal parameters w.r.t. matrix $\mathcal{H}$, and $\widehat{\sigma}_{f_i}^2 \in \mathbb{R}$, $\widehat{\sigma}_{\zeta_i}^2 \in \mathbb{R}$ and $\widehat{\Sigma}_{\varphi_i^{\mathrm{R}}} \in \mathbb{R}^{2r \times 2r}$ are the related covariance matrix estimates, obtained using consistent estimates of the respective sensitivity matrices and the sample covariance estimates of the data covariance (matrices). Consequently, thanks to the first-order Delta method, the asymptotic distribution of the modal parameter estimates can be approximated as Gaussian with

$$\widehat{f}_i \approx \mathcal{N}\left(f_i,\ \tfrac{1}{N}\widehat{\sigma}_{f_i}^2\right), \quad \widehat{\zeta}_i \approx \mathcal{N}\left(\zeta_i,\ \tfrac{1}{N}\widehat{\sigma}_{\zeta_i}^2\right), \quad \widehat{\varphi}_i^{\mathrm{R}} \approx \mathcal{N}\left(\varphi_i^{\mathrm{R}},\ \tfrac{1}{N}\widehat{\Sigma}_{\varphi_i^{\mathrm{R}}}\right).$$

The covariance related to the mode shape estimates can be propagated further onto MAC and MPC estimates, whose uncertainty quantification is recalled next.

4.2. Covariance of MAC estimate

Hereafter the index i is dropped for simplicity. Let φ and ψ be two complex-valued and independent mode shape vectors. The MAC computed between those vectors writes [44]

$$\mathrm{MAC}(\varphi, \psi) = \frac{|\varphi^H \psi|^2}{\varphi^H \varphi \psi^H \psi} = \frac{(\varphi^H \psi)(\psi^H \varphi)}{(\varphi^H \varphi)(\psi^H \psi)}. \tag{20}$$

The MAC is bounded between 0 and 1. A value of 1 indicates that φ and ψ are collinear, that is $\varphi = h\psi$ for some scalar $h \in \mathbb{C}$ since mode shapes are defined up to a constant. When φ is different from ψ the associated $\mathrm{MAC}(\varphi, \psi) \neq 1$, and the $\mathrm{MAC}(\varphi, \psi) = 0$ for (in practice unlikely) case of orthogonal mode shapes. The approach for uncertainty quantification of $\mathrm{MAC}(\widehat{\varphi}, \widehat{\psi})$ derived in [38] distinguishes two cases for approximating the asymptotic distribution of MAC estimates.

4.2.1. Gaussian approximation of $\mathrm{MAC}(\widehat{\varphi}, \widehat{\psi})$ *distribution*

When $\varphi \neq h\psi$ and $\mathrm{MAC}(\varphi, \psi)$ is strictly between 0 and 1, the distribution of $\mathrm{MAC}(\widehat{\varphi}, \widehat{\psi})$ can be approximated with a Gaussian function by means of the first-order Delta method. To illustrate this, define $\widehat{X} = \begin{bmatrix} \Re(\widehat{\varphi} - \varphi)^T & \Im(\widehat{\varphi} - \varphi)^T & \Re(\widehat{\psi} - \psi)^T & \Im(\widehat{\psi} - \psi)^T \end{bmatrix}^T$ and let the derivative of the MAC w.r.t. to

real and imaginary mode shape components be defined as $\mathcal{J}^{\mathrm{MAC}}_{\varphi,\psi} = \begin{bmatrix} \frac{\partial \mathrm{MAC}}{\partial \Re(\varphi)} & \frac{\partial \mathrm{MAC}}{\partial \Im(\varphi)} & \frac{\partial \mathrm{MAC}}{\partial \Re(\psi)} & \frac{\partial \mathrm{MAC}}{\partial \Im(\psi)} \end{bmatrix}$. Then, the first-order Taylor expansion of MAC writes

$$\mathrm{MAC}(\widehat{\varphi},\widehat{\psi}) \approx \mathrm{MAC}(\varphi,\psi) + \mathcal{J}^{\mathrm{MAC}}_{\varphi,\psi}\widehat{X} \ , \tag{21}$$

and the distribution of MAC estimates is approximated as

$$\mathrm{MAC}(\widehat{\varphi},\widehat{\psi}) \approx \mathcal{N}\left(\mathrm{MAC}(\varphi,\psi),\ \frac{1}{N}\widehat{\sigma}^2_{\mathrm{MAC}}\right), \tag{22}$$

where $\widehat{\sigma}^2_{\mathrm{MAC}} = \mathcal{J}^{\mathrm{MAC}}_{\widehat{\varphi},\widehat{\psi}}\widehat{\Sigma}_{\varphi^{\mathrm{R}},\psi^{\mathrm{R}}}(\mathcal{J}^{\mathrm{MAC}}_{\widehat{\varphi},\widehat{\psi}})^T$ is the estimate of the asymptotic variance of the MAC, $\mathcal{J}^{\mathrm{MAC}}_{\widehat{\varphi},\widehat{\psi}}$ is an estimate of the MAC derivative defined in [38], and $\widehat{\Sigma}_{\varphi^{\mathrm{R}},\psi^{\mathrm{R}}}$ contains the mode shape covariance estimates $\widehat{\Sigma}_{\varphi^{\mathrm{R}}}$ and $\widehat{\Sigma}_{\psi^{\mathrm{R}}}$ obtained from the chosen system identification method.

4.2.2. χ^2 approximation of $\mathrm{MAC}(\widehat{\varphi},\widehat{\psi})$ *distribution*

When $\widehat{\varphi}$ and $\widehat{\psi}$ estimate the same mode shape i.e., $\mathrm{MAC}(\varphi,\psi) = 1$, then the MAC derivative $\mathcal{J}^{\mathrm{MAC}}_{\varphi,\psi} = 0$, as shown in [38]. Then, the first-order Taylor series as in (21), is not sufficient to express $\mathrm{MAC}(\widehat{\varphi},\widehat{\psi})$ and hence the first-order Delta method is not adequate to approximate the distribution of MAC estimates. Following that, a second-order Taylor expansion of $\mathrm{MAC}(\widehat{\varphi},\widehat{\psi})$ writes

$$\mathrm{MAC}(\widehat{\varphi},\widehat{\psi}) \approx 1 + \tfrac{1}{2}\widehat{X}^T\mathrm{H}^{\mathrm{MAC}}_{\varphi,\psi}\ \widehat{X}, \tag{23}$$

where the Hessian $\mathrm{H}^{\mathrm{MAC}}_{\varphi,\psi} \in \mathbb{R}^{4r\times 4r}$ is the second derivative of $\mathrm{MAC}(\varphi,\psi)$ in φ and ψ, which was derived in detail in [38]. The asymptotic properties of $\mathrm{MAC}(\widehat{\varphi},\widehat{\psi})$ follow from (23) as

$$N(1-\mathrm{MAC}(\widehat{\varphi},\widehat{\psi})) \approx \widehat{X}^T_{\mathcal{N}}\overline{\mathrm{H}}^{\mathrm{MAC}}_{\varphi,\psi}\widehat{X}_{\mathcal{N}} = Q(\widehat{X}_{\mathcal{N}}) \ , \tag{24}$$

where $\overline{\mathrm{H}}^{\mathrm{MAC}}_{\varphi,\psi} = -\frac{1}{2}\,\mathrm{H}^{\mathrm{MAC}}_{\varphi,\psi}$, and $\widehat{X}_{\mathcal{N}} = \sqrt{N}\widehat{X} \approx \mathcal{N}(0,\Sigma_{\varphi^{\mathrm{R}},\psi^{\mathrm{R}}})$. Subsequently, $Q(\widehat{X}_{\mathcal{N}})$ describes a quadratic form of $\widehat{X}_{\mathcal{N}}$, which is related to the MAC estimate by the Hessian matrix $\overline{\mathrm{H}}^{\mathrm{MAC}}_{\varphi,\psi}$. The distribution of this quadratic form, and consequently the MAC estimate, can be approximated by estimating its first four cumulants, which are then used to obtain a scaled and shifted χ^2 distribution, as detailed in [38].

4.3. Covariance of MPC estimate

The MPC is a modal indicator used to determine the degree of complexity of a mode shape vector φ. It is defined as

$$\mathrm{MPC}(\varphi) = \frac{\left(\Re(\varphi)^T\Re(\varphi) - \Im(\varphi)^T\Im(\varphi)\right)^2 + 4(\Re(\varphi)^T\Im(\varphi))^2}{\left(\Re(\varphi)^T\Re(\varphi) + \Im(\varphi)^T\Im(\varphi)\right)^2}. \tag{25}$$

Similar to MAC, MPC is bounded between 0 and 1. For real-valued mode shapes its value is 1, and the lower the MPC the more complex-valued the mode shape is. Boundness of the MPC makes its uncertainty quantification with the first-order Delta method non-trivial, since the Gaussian function cannot approximate the distribution of its estimates when the underlying true value of MPC is at either 0 or 1 [37].

4.3.1. Gaussian approximation of $\mathrm{MPC}(\widehat{\varphi})$ distribution

In this section, the uncertainty quantification of MPC whose true values lie strictly between 0 and 1 is considered. Let the first-order derivative of the MPC w.r.t. to real and imaginary mode shape components be defined as $\mathcal{J}_\varphi^{\mathrm{MPC}} = \begin{bmatrix} \frac{\partial \mathrm{MPC}}{\partial \Re(\varphi)} & \frac{\partial \mathrm{MPC}}{\partial \Im(\varphi)} \end{bmatrix}$. Then, the first-order Taylor expansion of MPC estimate writes

$$\mathrm{MPC}(\hat{\varphi}) \approx \mathrm{MPC}(\varphi) + \mathcal{J}_\varphi^{\mathrm{MPC}} \begin{bmatrix} \Re(\hat{\varphi} - \varphi) \\ \Im(\hat{\varphi} - \varphi) \end{bmatrix}. \tag{26}$$

Its distribution can be approximated as Gaussian with the first-order Delta method [42] as

$$\mathrm{MPC}(\widehat{\varphi}) \approx \mathcal{N}\left(\mathrm{MPC}(\varphi),\ \frac{1}{N}\widehat{\sigma}^2_{\mathrm{MPC}}\right), \tag{27}$$

where $\widehat{\sigma}^2_{\mathrm{MPC}} = \mathcal{J}_\varphi^{\mathrm{MPC}}\widehat{\Sigma}_{\varphi^{\mathrm{R}}}(\mathcal{J}_\varphi^{\mathrm{MPC}})^T$ is the estimate of the asymptotic variance of the MPC and the detailed expression for $\mathcal{J}_\varphi^{\mathrm{MPC}}$ can be found in [37].

4.3.2. χ^2 approximation of $\mathrm{MPC}(\widehat{\varphi})$ distribution

In case MPC is obtained from asymptotically real-valued mode shape estimates i.e., its true value lies at 1, the Jacobian $\mathcal{J}_\varphi^{\mathrm{MPC}} = 0$ [37] and the first-order Taylor series as in (26) is not sufficient to express the related estimate of MPC. Following that, similar to the MAC obtained between estimates of equal mode shapes, a quadratic form of $\mathrm{MPC}(\widehat{\varphi})$ can be developed with a second-order Taylor expansion whose distribution can be approximated by estimating its first four cumulants, which are then used to obtain a scaled and shifted χ^2 distribution. For brevity, the derivation of the quadratic form of $\mathrm{MPC}(\widehat{\varphi})$ is hereby skipped and the interested reader is referred to [45] for more details.

4.4. Summary of the applied approaches

For uncertainty quantification of modal parameters and modal indicators, the subspace algorithms from Section 3 require derivation of the dedicated Jacobian matrices and each identification algorithm yields different statistical proprieties of the investigated parameters. An algorithmic summary is outlined below.

IOcov: Input/output covariance-driven algorithm (11), where $\mathcal{J}_{\mathcal{R}}^{\mathcal{H}_{\mathrm{IOcov}}}$ is computed after [28, Section 5.3.2.3] and the related sensitivity matrices are evaluated after [26, Algorithm 2],

IOdat: Input/output data-driven algorithm (12), where $\mathcal{J}_{\mathcal{R}}^{\mathcal{H}_{\mathrm{IOdat}}}$ is computed after [28, Section 5.3.2.1] and the related sensitivity matrices are evaluated after [26, Algorithm 2],

OOcov: Output-only covariance-driven algorithm (13), where $\mathcal{J}_{\mathcal{R}}^{\mathcal{H}_{\mathrm{Odat}}}$ is computed after [28, Section 5.3.1.1] and the related sensitivity matrices are evaluated after [26, Algorithm 2],

OOdat^a: Output-only data-driven algorithm (14), where $\mathcal{J}_{\mathcal{R}}^{\mathcal{H}_{\mathrm{Ocov}}}$ is computed after [28, Section 5.3.1.2] and the related sensitivity matrices are evaluated after [26, Algorithm 2],

OOdat^b: Output-only data-driven algorithm (14), where the sensitivity matrices are evaluated after [27].

The difference between OOdat^a and OOdat^b algorithms is the approach to obtain the estimates of (A, C). For OOdat^a algorithm, $(\widehat{A}, \widehat{C})$ are obtained from the shift invariance property of $\widehat{\mathcal{O}}$, and for OOdat^b algorithm $(\widehat{A}, \widehat{C})$ are obtained from the state regression.

5. Validation

This section presents a validation of the uncertainty quantification schemes outlined in Section 4.4. The validation is carried out on the measurement data from modal analysis of a 12.6 meter wind turbine blade [46], shown in Figure 1.

The modal analysis was conducted for the blade oriented with the leading edge facing downwards and supported with two elastic cord coils in the root and in the mid-section, as illustrated in Figure 1. An uncorrelated white noise excitation was exerted both in the flap-wise and the edge-wise directions by two Modal Exciter 100 shakers from Modal Shop, respectively fixed to the trailing edge and the leading edge mid span of the blade. The input force signals were generated in Siemens TestLab software and were measured by PCB mechanical impedance sensors attached between the structure and the stingers. The resultant vibration responses were measured with 19 PCB MEMS acceleration sensors. For modal analysis 19 measurement channels were used, i.e., 7 biaxial channels attached to the main axis of the blade, 1 biaxial and 1 uniaxial

channel located at the mid span of the trailing edge of the blade and 2 uniaxial channels located mid span of the leading edge of the blade. The biaxial sensors are measuring both the flap-wise and the edge-wise acceleration and the uniaxial sensors are measuring the flap-wise accelerations only. A detailed sensor layout is illustrated on Figure 2. Both input and output measurements were sampled with a frequency of 256 Hz for the period of 240 seconds. This experimental procedure was repeated 101 times, yielding 101 data sets, each comprising a set of input and output measurements of length $N = 61{,}600$. Prior to the modal parameter estimation data are decimated to 128 Hz. The modal parameters and their covariances are estimated for $p = 20$ at model order ranging from $20 - 100$ using the algorithms outlined in Section 4.4. The number of blocks used to obtain the sample covariance estimate of the data covariance matrix is equal to $n_b = 100$. The stabilization diagram of natural frequency estimates and their 95% confidence intervals obtained with the IOcov method is plotted together with the singular values of the cross power spectral density (CPSD) matrix evaluated for each frequency line [47, 48] on the left part of Figure 3.

To filter stabilization diagram from the modal parameter estimates that do not correspond to the physical modes of the blade, a threshold on the maximum Coefficient of Variation (CoV) [49] for the natural frequency equal to 2% and for the damping ratio equal to 20% is enforced, i.e., any mode whose CoV of the natural frequency exceeds 2% and 20% for the damping ratio, is discarded from the diagram on the left part of Figure 3. As a result, the non-physical mode estimates are discarded and modes of the blade are automatically extracted from the stabilization diagram. Other criteria for an automated analysis of the stabilization diagrams can also be used, see e.g., [5, 50]. A zoom on the natural frequency and the corresponding damping ratio estimates with their Delta method-based 95% confidence intervals is illustrated on the right part of Figure 3. It can be viewed that while the modal parameter estimates and the related confidence intervals depicted on the right part of Figure 3 differ for each model order, the majority of the estimates are contained by the confidence intervals of modal parameters obtained at different model orders, suggesting

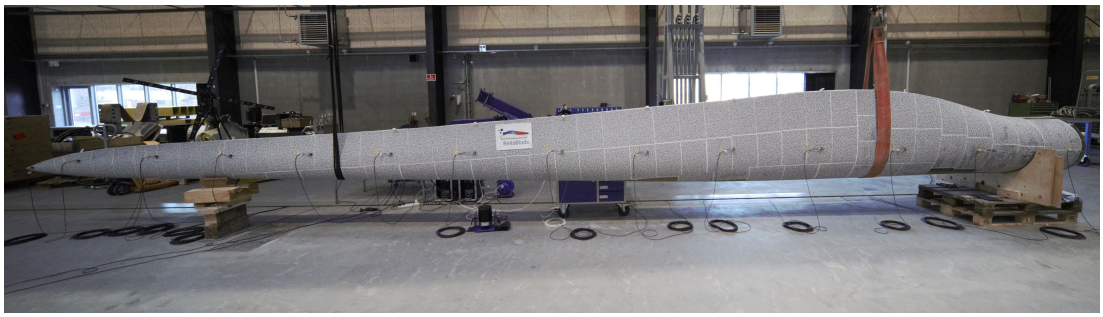

Figure 1: Wind turbine blade supported in a free-free boundary conditions on a test stand.

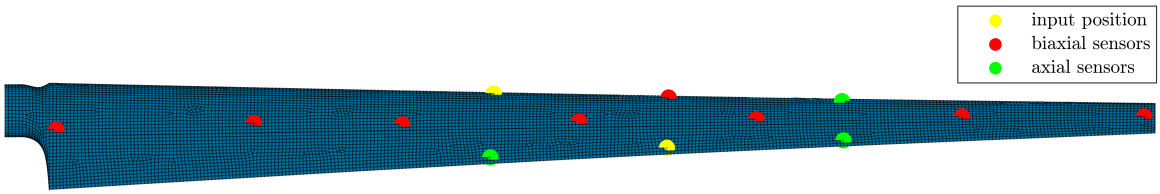

Figure 2: Sensor layout of the experimental setup.

that they are statistically equivalent and correspond to the same mode. Subsequently, the modal parameter estimates and their confidence intervals at model order 80 are selected and are tracked for each data set. Their averages obtained for the investigated subspace methods are depicted in Table 1. The eighth mode is close to the Nyquist frequency and its estimates are affected by the decimation. Thus, it is discarded from the study.

It can be viewed that while the average estimates of the natural frequency are very similar for all the in-

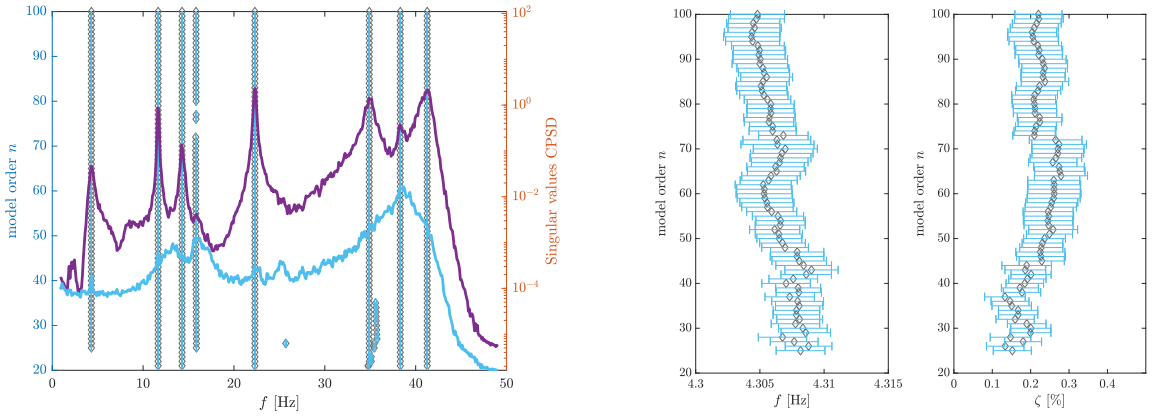

Figure 3: Stabilization diagram of the natural frequencies estimated from the first data set with IOcov algorithm (left). A zoom on the natural frequency and the corresponding damping ratio estimates with their Delta method-based 95% confidence intervals (right).

Table 1: Average estimates of the natural frequencies and the damping ratios obtained throughout the experimental campaign.

Algorithm/Mode		1	2	3	4	5	6	7
IOcov	$\bar{f}$ [Hz]	4.31	11.65	14.29	15.82	22.30	34.88	38.24
	$\bar{\zeta}$[%]	0.163	0.225	0.438	2.334	0.230	0.468	0.604
IOdat	$\bar{f}$ [Hz]	4.31	11.65	14.28	15.93	22.30	34.87	38.25
	$\bar{\zeta}$ [%]	0.206	0.224	0.473	2.652	0.232	0.485	0.595
OOcov	$\bar{f}$ [Hz]	4.26	11.66	14.31	15.88	22.31	34.99	38.25
	$\bar{\zeta}$ [%]	3.525	0.409	1.178	2.865	0.484	1.120	0.651
OOdat^a	$\bar{f}$ [Hz]	4.26	11.65	14.31	15.94	22.31	34.97	38.26
	$\bar{\zeta}$ [%]	2.975	0.395	1.194	2.603	0.495	1.415	0.603
OOdat^b	$\bar{f}$ [Hz]	4.25	11.66	14.30	15.93	22.31	34.93	38.26
	$\bar{\zeta}$ [%]	3.289	0.398	1.084	2.763	0.487	1.182	0.671

Table 2: Average variance estimates obtained from Delta method and empirical variances computed from the Monte Carlo.

Algorithm/Mode		1	2	3	4	5	6	7
IOcov	$\bar{\sigma}_f^{\mathrm{DM}}$ $\times 10^{-3}$ [Hz]	0.83	0.64	1.81	44.48	0.32	6.96	8.96
	σ_f^{MC} $\times 10^{-3}$ [Hz]	1.01	0.72	2.40	37.92	0.46	8.01	12.71
	$\bar{\sigma}_\zeta^{\mathrm{DM}}$ $\times 10^{-3}$ [%]	24.13	2.07	12.97	278.01	1.72	11.99	21.73
	$\sigma_\zeta^{\mathrm{MC}}$ $\times 10^{-3}$ [%]	23.22	2.23	14.02	364.72	2.06	17.62	27.45
IOdat	$\bar{\sigma}_f^{\mathrm{DM}}$ $\times 10^{-3}$ [Hz]	0.69	0.61	0.54	60.89	0.32	5.37	12.37
	σ_f^{MC} $\times 10^{-3}$ [Hz]	0.90	0.80	0.75	50.11	0.45	9.36	19.74
	$\bar{\sigma}_\zeta^{\mathrm{DM}}$ $\times 10^{-3}$ [%]	17.69	1.83	3.79	32.04	1.56	14.50	21.38
	$\sigma_\zeta^{\mathrm{MC}}$ $\times 10^{-3}$ [%]	19.03	1.72	4.28	35.20	1.97	20.16	25.64
OOcov	$\bar{\sigma}_f^{\mathrm{DM}}$ $\times 10^{-3}$ [Hz]	16.91	5.51	17.79	44.22	12.26	121.08	46.11
	σ_f^{MC} $\times 10^{-3}$ [Hz]	21.40	6.13	16.36	50.07	12.55	125.74	36.23
	$\bar{\sigma}_\zeta^{\mathrm{DM}}$ $\times 10^{-3}$ [%]	374.50	47.46	125.17	300.04	48.78	214.74	71.39
	$\sigma_\zeta^{\mathrm{MC}}$ $\times 10^{-3}$ [%]	363.95	42.82	100.86	335.99	49.42	173.84	70.40
OOdat[a]	$\bar{\sigma}_f^{\mathrm{DM}}$ $\times 10^{-3}$ [Hz]	14.68	5.27	12.01	32.34	9.56	96.99	18.15
	σ_f^{MC} $\times 10^{-3}$ [Hz]	15.96	6.09	13.37	39.72	10.22	121.28	23.19
	$\bar{\sigma}_\zeta^{\mathrm{DM}}$ $\times 10^{-3}$ [%]	288.92	45.40	85.70	193.05	42.22	243.85	45.51
	$\sigma_\zeta^{\mathrm{MC}}$ $\times 10^{-3}$ [%]	275.30	40.02	91.76	233.49	41.84	216.98	46.40
OOdat[b]	$\bar{\sigma}_f^{\mathrm{DM}}$ $\times 10^{-3}$ [Hz]	16.72	5.07	11.47	9.21	103.60	25.06	155.16
	σ_f^{MC} $\times 10^{-3}$ [Hz]	15.61	5.91	13.28	9.94	117.70	22.45	135.39
	$\bar{\sigma}_\zeta^{\mathrm{DM}}$ $\times 10^{-3}$ [%]	300.25	43.58	79.37	230.05	41.06	295.92	41.50
	$\sigma_\zeta^{\mathrm{MC}}$ $\times 10^{-3}$ [%]	297.45	37.78	84.13	265.69	42.78	221.79	47.61

vestigated algorithms, there are significant differences in the damping ratios obtained from the input/output and the output-only approaches. The true value of the damping ratio is unknown, however, the first mode damping estimates of a similar blade analyzed in [51] are close to input/output estimates from Table 1. Similar discrepancies in the damping ratio estimates from the input/output and the output-only methods were also reported in [52][53]. This can be possibly due to a shaker-structure interaction [54] or a bias stemming from the identification at a misspecified model order. It also suggests that the input/output identification methods are more accurate than the output-only algorithms, due to the additional information stemming from the knowledge about the inputs, which comes at the price of their availability [28, 55][4].

The Delta method-based variance estimate should correspond to the sample variance of the selected parameter. Denote σ^{MC} as the sample variance of a selected parameter and $\bar{\sigma}^{\mathrm{DM}} = \frac{1}{l}\sum_{j=1}^{l}\sigma^{\mathrm{DM,j}}$ as an average of Delta method-based variance $\sigma^{\mathrm{DM,j}}$, where $j = 1 \ldots l$ and l is the number of experimental data sets. The comparison of σ^{MC} and $\bar{\sigma}^{\mathrm{DM}}$ evaluated for the natural frequency and the damping ratio estimates is depicted in Table 2.

Few comments about the results presented in Table 2 are in place. First, it can be viewed that the variance of the natural frequency and the damping ratio estimates computed with the input/output subspace methods is lower than the corresponding variances obtained from the output-only methods. This stems from

Table 3: Average Delta method-based coefficients of variation of real and imaginary parts of the mode shape components and their experimental Monte Carlo equivalents.

Algorithm/Mode			1	2	3	4	5	6	7
IOcov	$\overline{\mathrm{CoV}}^{\mathrm{DM}}_{\Re(\varphi)}$	$\times 10^2$ [%]	0.086	0.061	0.088	0.029	0.083	0.037	0.031
	$\overline{\mathrm{CoV}}^{\mathrm{MC}}_{\Re(\varphi)}$	$\times 10^2$ [%]	0.079	0.056	0.084	0.049	0.097	0.023	0.029
	$\overline{\mathrm{CoV}}^{\mathrm{DM}}_{\Im(\varphi)}$	$\times 10^2$ [%]	3.593	2.058	3.113	4.125	1.872	0.747	0.911
	$\overline{\mathrm{CoV}}^{\mathrm{MC}}_{\Im(\varphi)}$	$\times 10^2$ [%]	3.217	1.297	3.024	4.279	2.294	1.041	0.947
IOdat	$\overline{\mathrm{CoV}}^{\mathrm{DM}}_{\Re(\varphi)}$	$\times 10^2$ [%]	0.069	0.072	0.089	0.089	0.104	0.029	0.030
	$\overline{\mathrm{CoV}}^{\mathrm{MC}}_{\Re(\varphi)}$	$\times 10^2$ [%]	0.059	0.069	0.094	0.073	0.095	0.021	0.031
	$\overline{\mathrm{CoV}}^{\mathrm{DM}}_{\Im(\varphi)}$	$\times 10^2$ [%]	3.990	4.525	3.512	5.298	3.253	1.344	1.142
	$\overline{\mathrm{CoV}}^{\mathrm{MC}}_{\Im(\varphi)}$	$\times 10^2$ [%]	3.874	3.922	3.771	5.761	2.880	1.061	1.121
OOcov	$\overline{\mathrm{CoV}}^{\mathrm{DM}}_{\Re(\varphi)}$	$\times 10^2$ [%]	0.263	0.053	0.262	0.054	0.233	0.295	0.274
	$\overline{\mathrm{CoV}}^{\mathrm{MC}}_{\Re(\varphi)}$	$\times 10^2$ [%]	0.249	0.046	0.373	0.039	0.393	0.342	0.312
	$\overline{\mathrm{CoV}}^{\mathrm{DM}}_{\Im(\varphi)}$	$\times 10^2$ [%]	1.572	3.919	1.430	6.589	7.521	8.723	7.712
	$\overline{\mathrm{CoV}}^{\mathrm{MC}}_{\Im(\varphi)}$	$\times 10^2$ [%]	1.505	2.069	1.534	7.367	8.812	9.564	8.596
OOdat^a	$\overline{\mathrm{CoV}}^{\mathrm{DM}}_{\Re(\varphi)}$	$\times 10^2$ [%]	0.307	0.197	0.476	0.116	0.712	0.377	0.287
	$\overline{\mathrm{CoV}}^{\mathrm{MC}}_{\Re(\varphi)}$	$\times 10^2$ [%]	0.272	0.257	0.434	0.097	0.829	0.295	0.259
	$\overline{\mathrm{CoV}}^{\mathrm{DM}}_{\Im(\varphi)}$	$\times 10^2$ [%]	1.738	4.800	3.530	1.245	7.363	8.762	8.412
	$\overline{\mathrm{CoV}}^{\mathrm{MC}}_{\Im(\varphi)}$	$\times 10^2$ [%]	1.410	3.842	3.660	0.927	8.100	6.935	7.531
OOdat^b	$\overline{\mathrm{CoV}}^{\mathrm{DM}}_{\Re(\varphi)}$	$\times 10^2$ [%]	0.139	0.021	0.189	0.037	0.193	0.088	0.081
	$\overline{\mathrm{CoV}}^{\mathrm{MC}}_{\Re(\varphi)}$	$\times 10^2$ [%]	0.123	0.026	0.204	0.039	0.204	0.097	0.084
	$\overline{\mathrm{CoV}}^{\mathrm{DM}}_{\Im(\varphi)}$	$\times 10^2$ [%]	2.445	3.668	3.433	5.504	8.264	4.643	5.133
	$\overline{\mathrm{CoV}}^{\mathrm{MC}}_{\Im(\varphi)}$	$\times 10^2$ [%]	2.583	4.222	3.078	5.954	8.437	6.373	6.778

the additional information given by the known inputs, which is also one of the conclusions of the simulation studies in [28][4]. Second, the difference in the variance obtained between the OOdat^a and the OOdat^b algorithms is small, suggesting that the choice of the method to obtain $(\widehat{A}, \widehat{C})$ has a small impact on the statistical errors on their estimates.

The covariance related to the mode shape estimates is investigated next. For this purpose an average CoV of their components is introduced. Recall that the mode shape estimates are defined up to a constant and for a statistical comparison in Monte Carlo experiment their components should be normalized. For this purpose, mode shapes are normalized by a component with the largest amplitude [25]. Let $\bar{\sigma}^{\mathrm{DM}}_{\Re(\varphi_c)} = \frac{1}{l}\sum_{j=1}^{l} \sigma^{\mathrm{DM,j}}_{\Re(\varphi_c)}$ and $\bar{\sigma}^{\mathrm{DM}}_{\Im(\varphi_c)} = \frac{1}{l}\sum_{j=1}^{l} \sigma^{\mathrm{DM,j}}_{\Im(\varphi_c)}$ be respectively the average Delta method-based standard deviation of the real and the imaginary $c = 1 \ldots r-1$ components of a mode shape, where $r-1$ denotes the number of mode shape components without the normalization component. Subsequently, let $\overline{\mathrm{CoV}}^{\mathrm{DM}}_{\Re(\varphi)} = \frac{1}{r-1}\sum_{c=1}^{r-1} \bar{\sigma}^{\mathrm{DM}}_{\Re(\varphi_c)}/\Re(\varphi_c)$ and $\overline{\mathrm{CoV}}^{\mathrm{DM}}_{\Im(\varphi)} = \frac{1}{r-1}\sum_{c=1}^{r-1} \bar{\sigma}^{\mathrm{DM}}_{\Im(\varphi_c)}/\Im(\varphi_c)$ be the average CoV of all the real and the imaginary mode shape components for a selected mode. Those quantities are compared against the experimental Monte Carlo-based $\overline{\mathrm{CoV}}^{\mathrm{MC}}_{\Re(\varphi)} = \frac{1}{r-1}\sum_{c=1}^{r-1} \sigma^{\mathrm{MC}}_{\Re(\varphi_c)}/\Re(\varphi_c)$ and $\overline{\mathrm{CoV}}^{\mathrm{MC}}_{\Im(\varphi)} = \frac{1}{r-1}\sum_{c=1}^{r-1} \sigma^{\mathrm{MC}}_{\Im(\varphi_c)}/\Im(\varphi_c)$ in Table 3.

It can be observed that the average CoV in Table 3 is approximately an order of magnitude smaller for the real parts of mode shape components than for their imaginary parts. This suggests that the standard deviation of the imaginary parts is relatively large in relation to the value of the component itself. This might indicate that the complexity of the investigated mode shapes is low and the related MPC values will approach 1. In addition to that, it can be viewed that the input-output identification algorithms yield smaller variation in the mode shape estimates than the output-only methods. This aligns well with the observations stemming from the results in Table 2.

The main outcome of both Table 2 and Table 3 is that the average Delta method-based quantities match the experimental Monte Carlo statistics quite well. For some modal parameter estimates, however, the average Delta method-based results are slightly mismatched. A detailed analysis of the validity of Delta method-based framework to approximate their distribution and to derive the related confidence intervals is investigated next.

5.1. Covariance related to the modal parameter estimates

In this section, a strategy to validate the statistical properties of the modal parameter estimates is devised. Firstly, the quality of the Gaussian approximation of the distribution of natural frequency, damping ratio and mode shape estimates is analyzed based on two-sample Kolmogorov-Smirnov test. Secondly, the correctness of the uncertainty quantification schemes for approximating the distribution of MAC and MPC estimates is analyzed.

5.1.1. Assessment of the Gaussian approximation of modal parameter estimates

The two-sample Kolmogorov-Smirnov test is a non-parametric test used to decide about the equality of two empirical cumulative probability distribution functions. In the context of validating Delta method-based variance estimates considered herein, the reference distribution is obtained empirically from the sample properties of the parameter estimates from the experimental Monte Carlo and the tested distribution is obtained using the variance obtained from Delta method. Subsequently, a decision about their equality is taken by comparing the value of test statistics to a quantile of the distribution of the test derived under the null hypothesis that the both sets of samples are drawn from the same distribution [56]. The quantile of the test distribution under the null hypothesis is evaluated for some confidence level α, where $1 - \alpha$ denotes the statistical significance level i.e., the probability of rejecting the null hypothesis, given that the null hypothesis is assumed to be true.

Let $\theta \in \mathcal{R}^l$ be a placeholder for a vector of a chosen parameter estimates e.g., the set of $j = 1 \dots l$ natural frequency, damping ratio or a chosen mode shape component estimates of the first mode, and let $\tilde{\theta} \in \mathcal{R}^l$ be centered and normalized θ, such that for each entry $j = 1 \dots l$

$$\tilde{\theta}_j = \left(\theta_j - \mu_\theta\right) / \sigma_\theta, \tag{28}$$

where μ_θ and σ_θ are respectively the mean and the standard deviation of θ. Assuming the Gaussian assumption for the distribution of θ, each $\tilde{\theta}_j$ follows a standard Gaussian distribution $\mathcal{N}(0, 1)$. Subsequently, let $F^{\mathrm{MC}}(\tilde{\theta})$ and $F^{\mathrm{DM}}(\tilde{\theta})$ be cumulative distribution functions of the modal parameter estimates normalized respectively by the variance of the considered Monte Carlo histogram and the corresponding variance obtained from Delta method. The $F^{\mathrm{DM}}(\tilde{\theta})$ is evaluated for each $j = 1 \dots l$ data set using Delta method-based standard deviation $\sigma^{\mathrm{DM,j}}$ and the sample mean of the considered parameter. Then, the Kolmogorov-Smirnov test is calculated as

$$S = \sup_{\tilde{\theta}} |F^{\mathrm{MC}}(\tilde{\theta}) - F^{\mathrm{DM}}(\tilde{\theta})|, \tag{29}$$

where the test statistics S boils down to a largest absolute difference between two cumulative distribution functions. Notice, that the two-sample test used herein does not assume that data are sampled from Gaussian distribution, or any other distribution [49]. For a decision that the Delta method-based distribution follows the sample distribution of the experimental Monte Carlo estimates, the test statistics S is compared to a quantile of the Kolmogorov distribution, where the type I error is set to 1%, i.e., the probability of rejecting the null hypothesis given it is true is 1%.

The two-sample Kolmogorov-Smirnov test is computed for each tracked modal parameter and the corresponding Delta method-based variance estimate. The ratio $T_{\tilde{\theta}}$ of the test statistics obtained from l data sets i.e., the average number of the test statistics satisfying the null hypothesis for the natural frequency and the damping ratio estimates is depicted in Table 4. For the mode shape estimates, the ratio $\overline{T}_{\tilde{\theta}}$ is presented as an average value of the test statistics ratio over all components. The ratio of 100% suggests that each standard deviation obtained with Delta method matches, in a statistical sense, to the standard deviation obtained empirically. On the contrary, the ratio of 0% suggests that none of Delta method-based standard deviations match their empirical counterparts. Results presented in Table 4 indicate that the distributions derived using the variance obtained with Delta method match the empirical distributions well. The average ratio of Kolmogorov-Smirnov test statistics satisfying the null hypothesis yields 86.57%, and for most of the cases the natural frequency and damping ratio estimates have higher scores than the average results

Table 4: Ratios of Kolmogorov-Smirnov test statistics for the natural frequency, the damping ratio and the mode shape component estimates.

Algorithm/Mode		1	2	3	4	5	6	7
IOcov	$\mathrm{T_f}$	100%	85.6%	78.5%	87.6%	69.4%	75.5%	82.1%
	T_ζ	100%	100%	88.4%	93.8%	68.9%	81.2%	78.6%
	$\overline{\mathrm{T}}_{\Re(\varphi)}$	99.0%	85.5%	81.5%	74.9%	81.8%	77.5%	71.6%
	$\overline{\mathrm{T}}_{\Im(\varphi)}$	89.1%	79.5%	78.9%	75.3%	92.4%	85.3%	83.1%
IOdat	$\mathrm{T_f}$	100%	81.6%	100%	85.8%	72.3%	92.1%	78.2%
	T_ζ	100%	100%	100%	67.8%	69.1%	59.1%	71.8%
	$\overline{\mathrm{T}}_{\Re(\varphi)}$	85.4%	89.4%	96.1%	82.4%	94.4%	81.9%	85.5%
	$\overline{\mathrm{T}}_{\Im(\varphi)}$	75.4%	87.4%	97.3%	77.1%	94.4%	89.7%	78.6%
OOcov	$\mathrm{T_f}$	98.8%	100%	93.9%	100%	99.0%	96.8%	93.8%
	T_ζ	98.8%	100%	90.9%	100%	100%	79.6%	93.8%
	$\overline{\mathrm{T}}_{\Re(\varphi)}$	85.5%	77.1%	73.5%	78.6%	81.8%	73.5%	77.1%
	$\overline{\mathrm{T}}_{\Im(\varphi)}$	91.6%	73.5%	80.1%	80.1%	77.1%	81.8%	75.4%
OOdat[a]	$\mathrm{T_f}$	100%	100%	100%	87.7%	100%	79.2%	99.0%
	T_ζ	100%	100%	100%	100%	100%	93.8%	99.0%
	$\overline{\mathrm{T}}_{\Re(\varphi)}$	91.6%	78.5%	70.3%	78.5%	65.3%	72.2%	73.9%
	$\overline{\mathrm{T}}_{\Im(\varphi)}$	86.0%	72.3%	74.2%	65.3%	65.3%	72.2%	65.3%
OOdat[b]	$\mathrm{T_f}$	96.9%	100%	100%	93.1%	100%	94.8%	99.0%
	T_ζ	98.9%	98.0%	98.0%	88.1%	99.0%	85.4%	99.0%
	$\overline{\mathrm{T}}_{\Re(\varphi)}$	99.6%	94.8%	86.7%	93.1%	93.1%	85.8%	85.8%
	$\overline{\mathrm{T}}_{\Im(\varphi)}$	93.1%	86.0%	70.8%	80.1%	86.1%	74.2%	78.5%

for the estimates of mode shape components. These results comply with the comparison of the empirical and Delta method-based standard deviations enclosed in Table 2. As expected, for the modal parameters whose Delta method-based standard deviation is far from the experimental one, the test statistics indicate that few Delta method-based distributions match the empirical distribution of the parameter. The average ratios of the test statistics for all mode shape components suggest that the Delta method-based fits for the low order mode shapes match the corresponding Monte Carlo distributions well. For the high order mode shapes, however, the average ratios are slightly mismatched. This possibly indicates that the uncertainty estimation might be less validated for the high order modes obtained at a high model order, which might be due to worse conditioning of the involved matrices for (pseudo-)inverting in the subspace methods [28].

The value of the test statistics S can be used as an empirical indicator for the quality assessment of the distribution matching. A small value of S indicates a small difference between the Monte Carlo-based and the Delta method-based cumulative distributions and their good fit, and a high value signifies a large difference between two tested cumulative distribution functions, which indicates that the distribution derived using the variance obtained from Delta method fits poorly to the empirical distribution. To illustrate an average outcome of the Delta method, the distribution fits corresponding to the mean value of the test statistics are shown in Figure 4.

As expected, the considered fits match the distributions of the natural frequency and the damping ratio

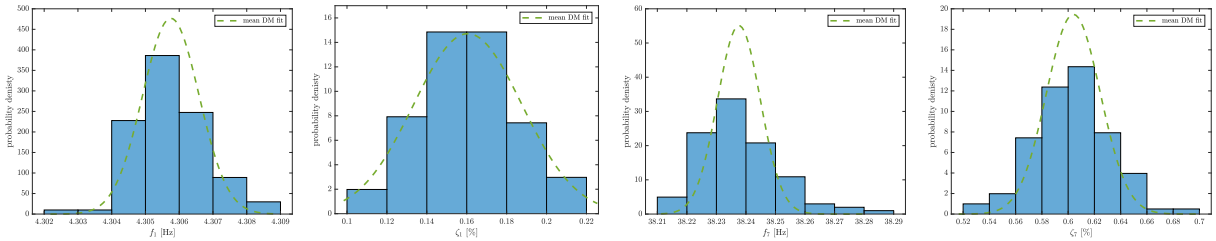

Figure 4: Histograms of the modal parameter estimates of the first and the seventh mode obtained from IOcov algorithm, together with the corresponding Delta method-based distribution fits. From the left: natural frequency of the first mode, damping ratio of the first mode, natural frequency of the seventh mode, damping ratio of the seventh mode.

estimates well. Equally good fits are expected for the low order mode shape components and slightly worse fits for the high order components. These results confirm that the variance of modal parameter estimates obtained from one data set using the first-order Delta method complies with the sample variance obtained from an exhaustive Monte Carlo experiment.

5.1.2. Assessment of the uncertainty quantification of MAC estimates

The distribution of MAC estimates depends on the geometric relation of the compared mode shapes. For estimates of different mode shapes, the corresponding MAC estimate lies strictly between 0 and 1, and is approximately Gaussian distributed, as recalled in Section 4.2.1. For estimates of the same mode shape, the MAC estimates accumulate at 1, and its distribution can be approximated by a shifted and scaled χ^2 function, as recalled in Section 4.2.2. Those two cases are considered herein. First, the Gaussian assumption for approximating the distribution of MAC estimated between two different mode shape estimates is validated. Second, the χ^2 approximation of the distribution of the MAC between estimates of the same mode shapes is empirically verified.

For the first case consider MAC calculated between the first and the second mode shape estimated from the same data set. For the second case consider MAC calculated between estimates of the same mode shape from different data sets. In the latter case the first MAC estimate is calculated between the same mode shape estimated from the first and the second data set, the second MAC estimate is calculated between the same mode shape estimated from the third and the fourth data set, and so on. For this purpose estimates of the mode shapes corresponding to the first and the third mode are considered. The empirical distributions of the aforementioned MAC estimates are depicted in Figure 5.

It can be observed that the histogram of MAC estimated between the different mode shapes is symmetric and the mean value of the histogram is in between 0 and 1. The histograms of MAC obtained from the estimates of the same mode shape accumulates close to 1 and its mass is skewed to the right.

Table 5: Ratios of Kolmogorov-Smirnov test statistics for MAC estimated between mode shapes corresponding to different modes.

Algorithm/Parameter	$T_{MAC_{12}}$	$T_{MAC_{13}}$	$T_{MAC_{14}}$	$T_{MAC_{15}}$	$T_{MAC_{16}}$	$T_{MAC_{17}}$
IOcov	83.2%	90.7%	94.1%	86.1%	52.9%	55.9%
IOdat	80.4%	98.9%	71.9%	74.3%	53.4%	57.6%
OOcov	83.1%	74.9%	89.2%	73.5%	50.2%	51.7%
OOdat^a	96%	82.3%	96%	89%	51.7%	56.7%
OOdat^b	96.9%	96.9%	97.9%	100%	52.1%	58.9%

Table 6: Ratios of Kolmogorov-Smirnov test statistics for MAC estimated between mode shapes corresponding to the same mode.

Algorithm/Parameter	$T_{MAC_{11}}$	$T_{MAC_{22}}$	$T_{MAC_{33}}$	$T_{MAC_{44}}$	$T_{MAC_{55}}$	$T_{MAC_{66}}$	$T_{MAC_{77}}$
IOcov	74.4%	68%	93.7%	84%	96.6%	56%	57.5%
IOdat	70%	90%	78%	64%	86%	70%	51.6%
OOcov	77.08%	82%	92.3%	68%	68%	57.0%	66.6%
OOdat^a	96%	54%	84.4%	57.5%	85.4%	72.4%	50%
OOdat^b	89.5%	100%	78%	54%	81.6%	68%	54%

Subsequently, both the Gaussian framework from Section 4.2.1 and the χ^2 framework from Section 4.2.2 are validated with using the two-sample Kolmogorov-Smirnov test. In case of the χ^2 approximation, the reference distribution is obtained after [57] from the cumulants of the empirical histogram. The resultant ratios $T_{\tilde{\theta}}$ of the test statistics are enclosed in Table 5 and Table 6 respectively for the Gaussian and the χ^2 approximations.

Table 5 shows that the ratio of test statistics for the MAC obtained from different mode shape estimates is larger than 50% for each of the considered MAC case, suggesting that the covariances obtained with Delta method are on average matching the empirical distribution of the investigated MAC. Similar conclusions can be drawn from Table 6, confirming the validity of the second-order Delta method to compute the cumulants needed to characterize the quadratic distribution, yielding similar distribution parameters as the full Monte Carlo histogram.

As a side comment, it can be viewed that on average the ratios of test statistics in Table 6 are lower,

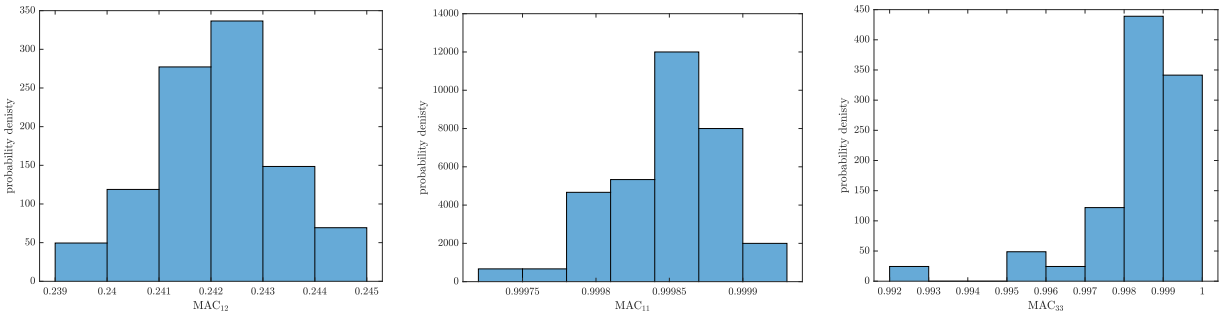

Figure 5: Histograms of MAC estimates obtained from the estimates of a different mode shape (left) and the estimates of the same mode shape (middle and right) using IOcov algorithm.

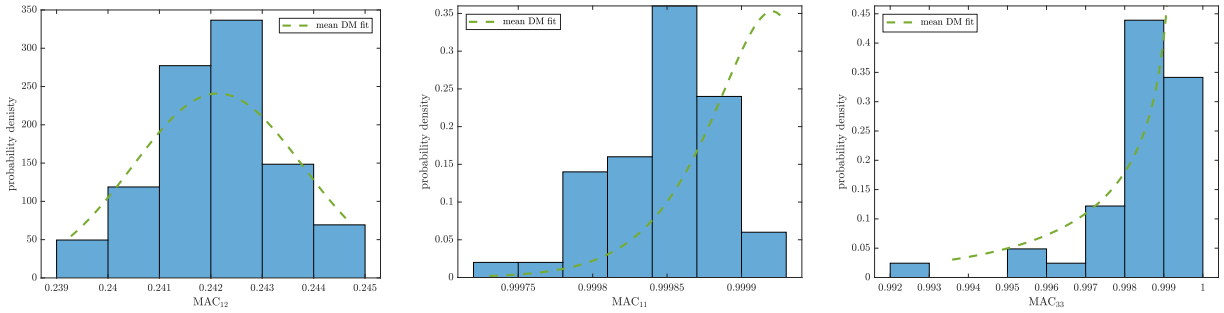

Figure 6: Histograms of MAC estimates obtained from the estimates of a different mode shape (left) and the estimates of the same mode shape (middle and right) using IOcov algorithm, together with the corresponding Delta method-based fits.

compared to the first-order results in Table 5. This can be explained by the fact that the second-order approximation of the quadratic form of MAC uses the first four cumunlants of the quadratic form to approximate the χ^2 distribution of MAC estimates, while the first-order Gaussian framework requires solely the first two cumulants (the mean and the covariance). The higher the order of the estimated cumulant, the larger tends to be its estimation variance [58], which results in higher accumulation of the statistical errors in the approximation of the distribution of MAC estimates. Also notice that the ratios of the Kolmogorov-Smirnov test statistics from Table 5 and Table 6 are lower for the last two MAC estimates when compared to the first five estimates. This is caused by the lower precision in the estimates of the sixth and the seventh mode shape, as indicated by the ratios related to the mode shape components enclosed in Table 4.

To conclude the MAC validation section, the mean Delta method-based fits corresponding to the mean value of the test statistics are shown in Figure 6.

It can be observed that the mean Delta method-based Gaussian fit to MAC_{12} and the mean shifted and scaled χ^2 fit to MAC_{33} match the empirical histograms well, which is supported by the high values of the test statistics ratios in Table 5 and Table 6. The mean shifted and scaled χ^2 fit to MAC_{11} is slightly mismatched, however it is expected that with larger sample sizes both the cumulants and the mode shape estimates will be estimated more precisely and the distribution fits will match the empirical histograms closer. This illustrates that the uncertainty quantification framework from Section 4.2 is, in practice, valid to obtain the distribution needed to characterize MAC computed for estimates of different and the same mode shapes.

5.1.3. Assessment of the uncertainty quantification of MPC estimates

Similar to the estimates of MAC, the distribution of MPC estimates is bounded between 0 and 1, which is related to the structural damping type. For non-proportionally damped modes, mode shapes are complex-

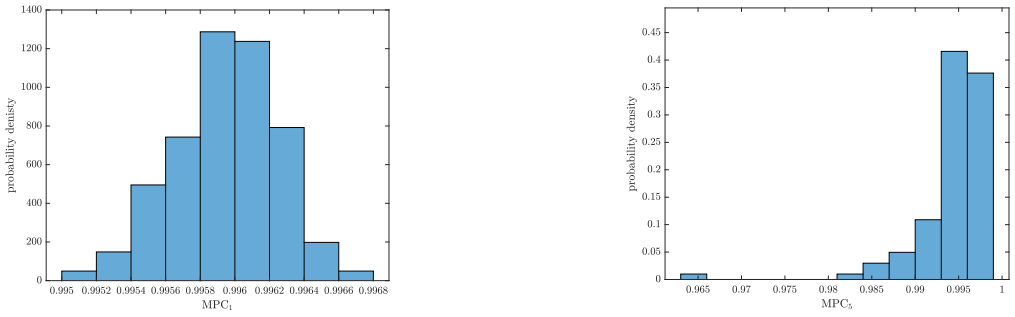

Figure 7: Histograms of MPC estimates obtained from the estimates of the first mode shape (left) and the estimates of the fifth mode shape (right) using IOcov algorithm.

valued vectors and the resulting MPC estimates are approximately Gaussian, as recalled in Section 4.1. For proportionally damped modes, mode shapes are real-valued vectors and the related MPC distribution can be approximated by a shifted and scaled χ^2 function, as proved in [45]. To show these two distribution types, consider MPC obtained for the mode shape estimates of the first and the fifth modes of the blade. Their histograms are showed in Figure 7.

While the MPC estimates are close to 1 in both cases, the histogram on the left part of Figure 7 is symmetric and resembles a Gaussian distribution, and the histogram on the right part of Figure 7 accumulates close to the distribution boarder and resembles a shifted and scaled χ^2 function. The latter can be a consequence of not only the proportional damping type but also errors in the mode shape estimates caused by a low sample size, as detailed in [37].

When no Monte Carlo histograms of MPC estimates are available, the choice between the Gaussian and the scaled and shifted χ^2 approximations needs to be made based on the MPC estimates and the related uncertainties. For this purpose, the decision framework from [38] can be adapted. In this particular validation study such Monte Carlo histograms are available. Consequently, they are used together with the ratios of Kolmogorov-Smirnov test statistic for the choice between the two uncertainty quantification frameworks.

First, consider a Gaussian validation as for the modal parameter estimates in Section 5.1.1. The ratio $T_{\tilde{\theta}}$ of the Kolmogorov-Smirnov test statistics satisfying the null hypothesis with the confidence level $\alpha = 99\%$ for MPC estimates is depicted in Table 7. Results from Table 7 suggest that the distributions calculated using the variances obtained from Delta method match well the empirical distribution of the MPC estimates for MPC_1, MPC_2, MPC_4 and MPC_6. The low values of $T_{\tilde{\theta}}$ for the MPC_3, MPC_5 and MPC_7 estimates suggests that the distributions obtained using Delta method-based variances mismatch the empirical distribution. In such a case, either the data length N has been too short for an adequate Gaussian approximation, or

Table 7: Ratios of Kolmogorov-Smirnov test statistics for MPC estimates- Gaussian fit case.

Algorithm/Parameter	T_{MPC_1}	T_{MPC_2}	T_{MPC_3}	T_{MPC_4}	T_{MPC_5}	T_{MPC_6}	T_{MPC_7}
IOcov	92.1%	84.9%	56.1%	86.7%	16.8%	72.4%	0%
IOdat	96.0%	96.0%	3.1%	78.5%	0%	67.6%	0%
OOcov	84.3%	77.2%	32.1%	61.2%	31.2%	65.1%	8.3%
OOdat^a	83%	71.3%	6.9%	79.4%	35.2%	66.5%	12.4%
OOdat^b	98.9%	98.0%	21.8%	99.0%	13.5%	89.1%	15.8%

Table 8: Ratios of Kolmogorov-Smirnov test statistics for MPC estimates- χ^2 fit case.

Algorithm/Parameter	T_{MPC_3}	T_{MPC_5}	T_{MPC_7}
IOcov	77.4%	62.6%	62.4%
IOdat	74.5%	72.4%	75.6%
OOcov	87.4%	63.4%	51.5%
OOdat^a	89.1%	95.8%	55.6%
OOdat^b	94.1%	96.9%	36.4%

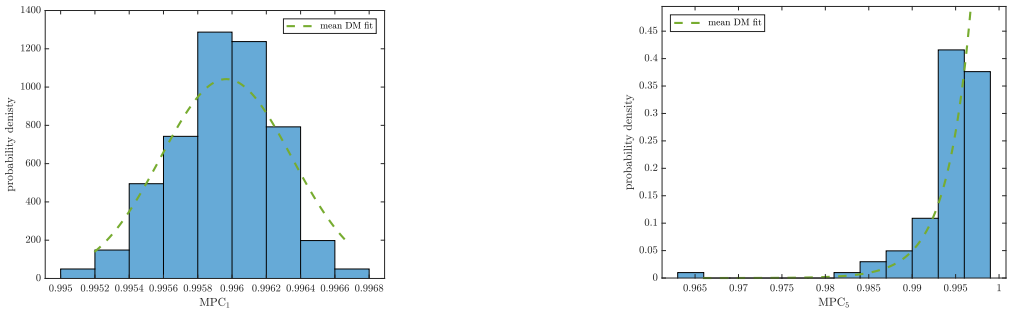

Figure 8: Histograms of MPC estimates obtained from the estimates of the first mode shape (left) and the estimates of the fifth mode shape (right) using IOcov algorithm, together with the corresponding Delta method-based distribution fits.

the underlying mode shape is not complex-valued but real-valued. In the latter case, the first-order Delta method reaches its limits, and the second-order Delta method after Section 4.3.2 and [45] is deployed to approximate the distribution of the related MPC estimates. The ratio $T_{\tilde{\theta}}$ of the test statistics for the MPC obtained from the third, the fifth and the seventh mode shape estimates is depicted in Table 8.

As expected, the ratios of test statistics obtained with the second-order approximation in Table 8 are higher for MPC_3, MPC_5 and MPC_7 than the corresponding ratio in Table 7. This indicates that the corresponding mode shapes are likely an asymptotically real-valued vectors.

The mean fits corresponding to the mean value of the test statistics are shown in Figure 8. It can be observed that, the mean first-order Delta method-based distribution fit matches the empirical histogram of MPC_1 estimates well. This confirms the validity of the Gaussian approximation for MPC_1 and suggests that the corresponding mode shapes are most likely complex-valued. The shifted and scaled χ^2 fit is adequate to characterize the shape of the MPC histogram accumulating close to the distribution border at 1. This confirms that the second-order Delta method framework and the shifted and scaled χ^2 distribution is capable

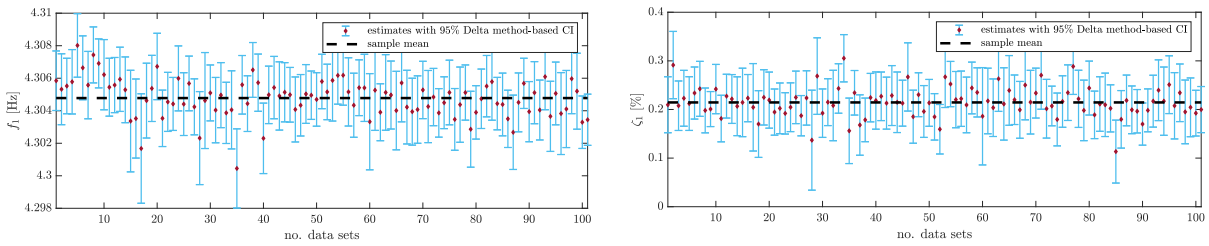

Figure 9: First-order Delta method-based 95% confidence intervals of the natural frequency and the damping ratio estimates with the sample mean of the respective parameters.

of approximating the distribution of the estimates of MPC_5 and suggests that the corresponding mode shapes are most likely real-valued.

5.2. Validation of the confidence intervals obtained from Delta method

The practical application of the uncertainty quantification algorithms investigated in the previous section is, however, not to establish a distribution function, but to estimate the corresponding confidence intervals (CIs). Therefore to finalize the validation, the CIs are obtained for both the modal parameter and the modal indicator estimates and their merit is studied based on the empirical statistics obtained from the blade experiment.

Two frameworks for uncertainty quantification considered in this paper require establishing separate validation cases. First, consider Guassian CIs obtained with the first-order Delta method. These intervals are centered around the parameter estimates and with some confidence level α contain the true value of the considered parameter i.e., for $\alpha = 95\%$, at least 95% of the confidence intervals encompass its true value [59]. To validate this, assume that the sample mean obtained from all the estimates of the chosen parameter is close to its expected value. Then, around 95% of Gaussian CIs should contain the sample mean of the considered parameter. The Delta method-based CIs obtained with IOcov algorithm for the estimates of the natural frequency and the damping ratio of the first mode are illustrated in Figure 9. The percentage of the CIs containing the sample mean of the natural frequency, the damping ratio and the mode shape estimates is enclosed in Table 9. For the mode shape components, the related percentage is calculated as an average over all the components. The validation results of Gaussian CIs for the MAC and the MPC estimates are similar as for the modal parameter estimates and are omitted here for brevity.

The average percentage of the CIs containing the sample mean of the natural frequency and the damping ratio estimates is 82.33% and of the mode shape components estimates is 98.89% for the input/output methods, and 94.81% and 93.83% respectively for the output-only algorithms. The slightly low score for the

Table 9: Percentage of the Delta method-based CIs containing the sample mean of the natural frequency, the damping ratio and the mode shape component estimates.

Algorithm/Mode		1	2	3	4	5	6	7
IOcov	f	94.0%	89.3%	75.2%	89.6%	84.2%	80.2%	72.8%
	ζ	94.1%	97.0%	93.1%	92.8%	79.3%	80.2%	76.9%
	$\Re(\varphi)$	98.6%	100%	100%	99.4%	100%	94.4%	99.9%
	$\Im(\varphi)$	99.5%	100%	99.9%	99.7%	100%	94.9%	100%
IOdat	f	88.1%	84.5%	75.7%	71.4%	74.5%	73.8%	51.9%
	ζ	96.0%	98.0%	87.1%	77.6%	81.7%	85.5%	60.4%
	$\Re(\varphi)$	100%	100%	95.9%	92.3%	100%	100%	100%
	$\Im(\varphi)$	100%	100%	99.9%	94.8%	100%	100%	100%
OOcov	f	93.9%	99.0%	94.9%	94.9%	100%	94.6%	93.8%
	ζ	100%	100%	96.9%	94.9%	99.0%	100%	97.9%
	$\Re(\varphi)$	100%	100%	100%	96.7%	100%	100%	100%
	$\Im(\varphi)$	100%	100%	100%	100%	100%	100%	100%
OOdat[a]	f	95%	98.0%	93.1%	94.5%	99.0%	93.8%	86.1%
	ζ	99%	100%	95.1%	97.3%	99.0%	97.9%	98.0%
	$\Re(\varphi)$	100%	100%	97.7%	96.5%	100%	100%	99.9%
	$\Im(\varphi)$	100%	100%	99.2%	94.8%	100%	100%	100%
OOdat[b]	f	100%	98.0%	93.1%	89.8%	98.0%	97.9%	91.1%
	ζ	98.9%	100%	93.8%	93.2%	98.0%	97.9%	96.0%
	$\Re(\varphi)$	98.6%	90.8%	94.8%	97.3%	96.8%	99.1%	95.1%
	$\Im(\varphi)$	75.9%	64.3%	92.7%	93%	68.6%	62.6%	78.9%

input/output methods can be explained by a lower accuracy in estimating the parameters of the seventh mode. The high scores for the mode shape components and the output-only algorithms show that even if the empirical distributions are not always perfectly matching the first-order Delta method-based approximations, as suggested by the ratio of the Kolmogorov-Smirnov test statistics in Table 4, the computed confidence intervals are quite accurate.

Second, the Delta method-based quantiles of the shifted and scaled χ^2 distribution are examined in the context of MAC and MPC estimates. Recall that in the Gaussian case, the computed CIs are centered around the estimate and describe with some confidence level a plausible range for the *true value* of the considered parameter. In the case of the scaled and shifted χ^2 approximation of the distribution of MAC and MPC estimates, the true value of either parameters is already known and equal to 1. Therefore it is not practical to define a confidence interval around the estimate to encompass the true value of the considered parameter, as its true value is assumed to be known. Instead, the related quantile is defined starting from the parameter true value at the distribution boarder at 1 to contain a plausible range of the parameter estimates. Such 95% quantiles are obtained for the MAC_{11} estimates validated previously in Section 5.1.2 and the MPC_3 estimates from Section 5.1.3, and shown in the respective parts in Figure 10. To validate these intervals, it is checked how many of the related estimates of MAC and MPC lie within their bounds. Percentage of the estimates of MAC and MPC indicators contained in the 95% intervals of the shifted and

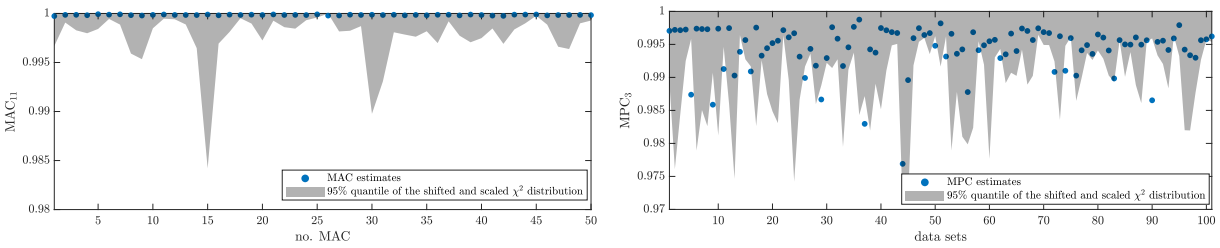

Figure 10: Second-order Delta method-based 95% quantiles of the shifted and scaled χ^2 approximation of MAC and MPC distribution.

Table 10: Percentage of the 95% shifted and scaled χ^2 distribution quantiles containing the MAC computed between the estimates of equal mode shapes.

Algorithm/Parameter	MAC_{11}	MAC_{22}	MAC_{33}	MAC_{44}	MAC_{55}	MAC_{66}	MAC_{77}
IOcov	100%	100%	100%	74%	100%	86%	98%
IOdat	100%	100%	100%	58.5%	100%	100%	94%
OOcov	100%	100%	100%	80.9%	100%	78%	94%
OOdat^a	98%	74%	100%	54%	100%	100%	80%
OOdat^b	100%	68.8%	94%	54%	94%	97.7%	78%

Table 11: Percentage of the 95% shifted and scaled χ^2 distribution quantiles containing the MPC computed from the estimates of real mode shapes.

Algorithm/Parameter	MPC_3	MPC_5	MPC_7
IOcov	82.2%	92.1%	65.5%
IOdat	95.1%	100%	75.4%
OOcov	100%	95.7%	70.7%
OOdat^a	97.1%	81.2%	61.4%
OOdat^b	92.1%	98.9%	46.5%

scaled χ^2 approximation of MAC and MPC distributions are enclosed respectively in Table 10 and Table 11.

High percentage of MAC estimates within the 95% quantiles suggests that the related shifted and scaled χ^2 distribution possibly slightly overestimates the distribution of MAC estimates, which can also be conjectured from the distribution fits in Figure 6. Despite obtained using the second-order statistics, the quantiles of the MAC and MPC distribution approximation are quite accurate and for most of the cases contain majority of the related estimates.

6. Conclusions

In this paper, an extensive case study validating the statistical Delta method-based framework to obtain the distribution characteristics of the modal parameter and the modal indicator estimates was presented for several subspace algorithms. The input/output subspace methods exhibited lower variances in modal parameter estimates than the output-only methods. Methods to obtain the estimates of (A, C) i.e., the

shift invariance and the state regression, were found to have no significant influence on the covariance of estimated parameters. The results confirmed that the statistical properties of the modal parameter estimates obtained from one data set with the first-order Delta method are, on average, equivalent to the empirical statistics obtained from the Monte Carlo experiment. It was also shown that for most of the estimates the first-order Delta method-based confidence intervals are accurate and contain the Monte Carlo mean of the estimated parameter. Although some second-order Delta method distribution fits were slightly mismatched with the histograms of MAC between equal mode shape estimates and MPC of asymptotically real-valued mode shapes, it is expected that with larger sample sizes, the variance errors on the estimated parameters and the higher order cumulants of the distribution approximating MAC and MPC estimates will decrease, and the second-order Delta method-based distribution characteristics will match their empirical equivalents better.

Acknowledgments

The experimental work has been conducted with the equipment from Villum Center for Advanced Structural and Material Testing (CASMaT). The support from Villum Fonden (Award ref. 00007293) is gratefully acknowledged. This work is also supported by the Danish Energy Agency through the Energy Technology Development and Demonstration Program (EUDP), Grant No. 64018-0068, with the supporting project ReliaBlade. The related support is greatly appreciated.

References

[1] L. Ljung, System Identification (2Nd Ed.): Theory for the User, Prentice Hall PTR, Upper Saddle River, NJ, USA, 1999.

[2] R. Pintelon, J. Schoukens, System identification: a frequency domain approach, John Wiley & Sons, 2012.

[3] P. van Overschee, B. de Moor, Subspace Identification for Linear Systems, 1st Edition, Springer, 1996.

[4] E. Reynders, System identification methods for (operational) modal analysis: Review and comparison, Archives of Computational Methods in Engineering 19 (1) (2012) 51–124.

[5] E. Reynders, J. Houbrechts, G. De Roeck, Fully automated (operational) modal analysis, Mechanical Systems and Signal Processing 29 (2012) 228–250.

[6] B. Peeters, G. De Roeck, Stochastic system identification for operational modal analysis: a review, J. Dyn. Sys., Meas., Control 123 (4) (2001) 659–667.

[7] B. Peeters, G. de Roeck, Reference-based stochastic subspace identification for output-only modal analysis, Mechanical Systems and Signal Processing 13 (6) (1999) 855 – 878.

[8] J. Brownjohn, F. Magalhaes, E. Caetano, A. Cunha, Ambient vibration re-testing and operational modal analysis of the humber bridge, Engineering Structures 32 (8) (2010) 2003–2018.

[9] F. Magalhães, Á. Cunha, Explaining operational modal analysis with data from an arch bridge, Mechanical Systems and Signal Processing 25 (5) (2011) 1431 – 1450.

[10] S. Greś, M. Döhler, P. Andersen, L. Mevel, Kalman filter-based subspace identification for operational modal analysis under unmeasured periodic excitation, Mechanical Systems and Signal Processing 146 (2021) 106996.

[11] S. Pereira, E. Reynders, F. Magalhães, Á. Cunha, J. P. Gomes, The role of modal parameters uncertainty estimation in automated modal identification, modal tracking and data normalization, Engineering Structures 224 (2020) 111208.

[12] S. Diord, F. Magalhães, Á. Cunha, E. Caetano, N. Martins, Automated modal tracking in a football stadium suspension roof for detection of structural changes, Structural Control and Health Monitoring 24 (11) (2017) e2006.

[13] R. Riva, S. Cacciola, A. Croce, High-resolution periodic mode shapes identification for wind turbines, Vol. 1037, 2018, p. 062002.

[14] F. Ubertini, C. Gentile, A. L. Materazzi, Automated modal identification in operational conditions and its application to bridges, Engineering Structures 46 (2013) 264–278.

[15] S. Greś, M. Fejerskov, L. Ibsen, L. Damkilde, Experimental damping assessment of a full scale offshore mono bucket foundation, in: P. Sas, D. Moens, A. van de Walle (Eds.), Proceedings of ISMA2016, KU Leuven, Department of Mechanical Engineering, PMA, 2016, pp. 4045–4054.

[16] D. Bauer, M. Deistler, W. Scherrer, Consistency and asymptotic normality of some subspace algorithms for systems without observed inputs, Automatica 35 (7) (1999) 1243 – 1254.

[17] A. Benveniste, L. Mevel, Nonstationary consistency of subspace methods, IEEE Transactions on Automatic Control 52 (6) (2007) 974–984.

[18] M. Döhler, L. Mevel, Fast multi-order computation of system matrices in subspace-based system identification, Control Engineering Practice 20 (9) (2012) 882 – 894.

[19] M. Verhaegen, Subspace model identification part 3. analysis of the ordinary output-error state-space model identification algorithm, International Journal of Control 58 (3) (1993) 555–586.

[20] M. Viberg, B. Wahlberg, B. Ottersten, Analysis of state space system identification methods based on instrumental variables and subspace fitting, Automatica 33 (9) (1997) 1603 – 1616.

[21] D. Bauer, M. Jansson, Analysis of the asymptotic properties of the MOESP type of subspace algorithms, Automatica 36 (4) (2000) 497 – 509.

[22] M. Jansson, Asymptotic variance analysis of subspace identification methods, IFAC Proceedings Volumes 33 (15) (2000) 91 – 96, 12th IFAC Symposium on System Identification (SYSID 2000), Santa Barbara, CA, USA, 21-23 June 2000.

[23] A. Chiuso, G. Picci, The asymptotic variance of subspace estimates, Journal of Econometrics 118 (1) (2004) 257 – 291.

[24] R. Pintelon, P. Guillaume, J. Schoukens, Uncertainty calculation in (operational) modal analysis, Mechanical Systems and Signal Processing 21 (6) (2007) 2359 – 2373.

[25] E. Reynders, R. Pintelon, G. De Roeck, Uncertainty bounds on modal parameters obtained from stochastic subspace identification, Mechanical Systems and Signal Processing 22 (4) (2008) 948 – 969.

[26] M. Döhler, L. Mevel, Efficient multi-order uncertainty computation for stochastic subspace identification, Mechanical Systems and Signal Processing 38 (2) (2013) 346–366.

[27] E. P. Reynders, Uncertainty quantification in data-driven stochastic subspace identification, Mechanical Systems and Signal Processing 151 (2021) 107338.

[28] P. Mellinger, M. Döhler, L. Mevel, Variance estimation of modal parameters from output-only and input/output subspace-

based system identification, Journal of Sound and Vibration 379 (C) (2016) 1 – 27.

[29] E. Reynders, R. Pintelon, G. De Roeck, Consistent impulse-response estimation and system realization from noisy data, IEEE Transactions on Signal Processing 56 (7) (2008) 2696–2705.

[30] S. Greś, M. Döhler, N.-J. Jacobsen, L. Mevel, Uncertainty quantification of input matrices and transfer function in input/output subspace system identification, Mechanical Systems and Signal Processing 167 (2022) 108581.

[31] M. Döhler, F. Hille, L. Mevel, W. Rücker, Structural health monitoring with statistical methods during progressive damage test of s101 bridge, Engineering Structures 69 (2014) 183 – 193.

[32] S. Greś, M. Döhler, L. Mevel, Statistical model-based optimization for damage extent quantification, Mechanical Systems and Signal Processing 160 (2021) 107894.

[33] C. Argyris, C. Papadimitriou, P. Panetsos, P. Tsopelas, Bayesian model-updating using features of modal data: Application to the metsovo bridge, Journal of Sensor and Actuator Networks 9 (2) (2020) 27.

[34] G. Steenackers, P. Guillaume, Finite element model updating taking into account the uncertainty on the modal parameters estimates, Journal of Sound and Vibration 296 (4) (2006) 919 – 934.

[35] M. Friswell, J. E. Mottershead, Finite element model updating in structural dynamics, Vol. 38, Springer Science & Business Media, 2013.

[36] E. Simoen, G. De Roeck, G. Lombaert, Dealing with uncertainty in model updating for damage assessment: A review, Mechanical Systems and Signal Processing 56 (2015) 123–149.

[37] S. Greś, M. Döhler, P. Andersen, L. Mevel, Uncertainty quantification for the modal phase collinearity of complex mode shapes, Mechanical Systems and Signal Processing 152 (2021) 107436.

[38] S. Greś, M. Döhler, L. Mevel, Uncertainty quantification of the modal assurance criterion in operational modal analysis, Mechanical Systems and Signal Processing 152 (2021) 107457.

[39] E. Reynders, K. Maes, G. Lombaert, G. D. Roeck, Uncertainty quantification in operational modal analysis with stochastic subspace identification: Validation and applications, Mechanical Systems and Signal Processing 66-67 (2016) 13 – 30.

[40] R. Bitmead, Persistence of excitation conditions and the convergence of adaptive schemes, IEEE Transactions on Information Theory 30 (2) (1984) 183–191.

[41] P. van Overschee, B. de Moor, N4SID: Subspace algorithms for the identification of combined deterministic-stochastic systems, Automatica 30 (1) (1994) 75 – 93.

[42] G. Casella, R. L. Berger, Statistical Inference, 2nd Edition, Cengage Learning, 2001.

[43] E. J. Hannan, Multiple time series, Vol. 38, John Wiley & Sons, 2009.

[44] R. J. Allemang, The modal assurance criterion (MAC): Twenty years of use and abuse, Journal of Sound and Vibration 37.

[45] S. Greś, Vibration-based monitoring of structures: algorithms for fault detection and uncertainty quantification of modal indicators, Ph.D. thesis (2019).

[46] P. U. Haselbach, S. Semenov, P. Berring, DTU's blade research and demonstration platform, IOP Conference Series: Materials Science and Engineering 942 (2020) 012043.

[47] R. Brincker, L. Zhang, P. Andersen, Output-only modal analysis by frequency domain decomposition, in: P. Sas, D. Moens (Eds.), Proceedings of ISMA25, Katholieke Universiteit, Leuven, 2000, pp. 717–723.

[48] A. Brandt, Noise and vibration analysis: signal analysis and experimental procedures, John Wiley & Sons, 2011.

[49] B. S. Everitt, A. Skrondal, The cambridge dictionary of statistics.

[50] V. Yaghoubi, M. K. Vakilzadeh, T. J. Abrahamsson, Automated modal parameter estimation using correlation analysis and bootstrap sampling, Mechanical Systems and Signal Processing 100 (2018) 289–310.

[51] M. M. Łuczak, R. Riva, S. C. Yeniceli, S. H. Madsen, E. Di Lorenzo, Identification of the test setup influence on the modal properties of a short wind turbine blade during fatigue test, Measurement 174 (2021) 108960.

[52] Á. Cunha, J. Gomes, S. Pereira, F. Magalhães, J. Lemos, Input-output vs output-only modal identification of baixo sabor concrete arch dam, in: 9th European Workshop on Structural Health Monitoring, 2018.

[53] P. Mellinger, M. Döhler, L. Mevel, Variance estimation of modal parameters from input/output covariance-driven subspace identification, in: ISMA - 27th Conference on Noise and Vibration Engineering, Leuven, Belgium, 2016.

[54] G. ZHANG, X. WANG, Z. YANG, Study on excitation force characteristics in a coupled shaker-structure system considering structure modes coupling, Chinese Journal of Aeronautics.

[55] L. Mevel, A. Benveniste, M. Basseville, M. Goursat, B. Peeters, H. V. der Auweraer, A. Vecchio, Input/output versus output-only data processing for structural identification-application to in-flight data analysis, Journal of Sound and Vibration 295 (3) (2006) 531 – 552.

[56] G. Marsaglia, W. W. Tsang, J. Wang, Evaluating kolmogorov's distribution, Journal of Statistical Software, Articles 8 (18).

[57] H. Liu, Y. Tang, H. H. Zhang, A new chi-square approximation to the distribution of non-negative definite quadratic forms in non-central normal variables, Computational Statistics and Data Analysis 53 (4) (2009) 853 – 856.

[58] D. Mämpel, A. K. Nandi, Robust Cumulant Estimation, Springer US, Boston, MA, 1999, pp. 253–277.

[59] J. Neyman, H. Jeffreys, Outline of a theory of statistical estimation based on the classical theory of probability, Philosophical Transactions of the Royal Society of London. Series A, Mathematical and Physical Sciences 236 (767) (1937) 333–380.